ISSN: 0975-8585

Research Journal of Pharmaceutical, Biological and Chemical Sciences

DFT and Docking Studies of the Relationships between Electronic Structure and 5-HT_{2A} Receptor Binding Affinity in N-Benzylphenethylamines.

Juan S. Gómez-Jeria* and Andrés Robles-Navarro.

Quantum Pharmacology Unit, Department of Chemistry, Faculty of Sciences, University of Chile. Las Palmeras 3425, Santiago 7800003, Chile.

ABSTRACT

An extensive study was carried out to find formal relationships between electronic structure and 5-HT_{2A} receptor binding affinity in a family of 44 N-benzylphenethylamines. These molecules were also docked to a structure of a new model of the 5-HT_{2A} receptor. The QSAR results detected several atoms involved in the binding with HT_{2A}. For the first time a local atomic reactivity index related to the 4-substituent (important in the psychoactive effects of 2,5-dimethoxy-4-X-phenylethylamines and 2,5-dimethoxy-4-X-amphetamines) appeared in the QSAR results. Docking results show that molecules seem to have different modes of binding to this receptor. A given moiety of the molecules is able to interact with more than one residue of the receptor and not all the time a certain moiety interacts with the same residue.

Keywords: 5-HT_{2A} receptor, QSAR, DFT, serotonin, binding affinity, docking, *N*-benzylphenethylamines, chemical reactivity.

Corresponding author

ISSN: 0975-8585

INTRODUCTION

Hallucinogens based of the 2,5-dimethoxy-4-X-phenylethylamine (2C family) and 2,5-dimethoxy-4-X-amphetamine skeletons (X=OMe, Br, Me, etc.) are very well known chemicals having distinct psychoactive activities [1, 2]. The attachment of an N-benzyl derivative has produced a new family of very potent psychoactive molecules. The first one, 2-(4-iodo-2,5-dimethoxyphenyl)-*N*-[(2-methoxyphenyl) methyl] ethanamine (25I-NBOMe, 25I) was discovered in 2003 and seems to have entered into the illegal drug market around 2010. Being more potent that LSD, sometimes is sold as such. Today there are few doubts that 25I-NBOMe is the causative agent of an increasing number of severe intoxications and deaths [3-11]. It seems that some mind effects of its consumption are notably different of LSD. These molecules exert their psychoactive actions by binding to the 5-HT_{2A} receptor. Our research on the structure-activity of similar compounds began in 1984 [12-20]. Recently we have carried out a study of the docking of some hallucinogens to the 5-HT_{2A} receptor [21]. The main conclusion of this study is the necessity of carrying out QSAR and docking studies in large series of molecules. A Thesis published the receptor binding affinity values of a group of a large group of 48 N-Benzylphenethylamines [22]. With part of these molecules (44) we performed formal structure-receptor binding affinity and docking studies for the 5-HT_{2B} receptor case [23]. In this paper we present the results of a study of the relationship between electronic structure and 5-HT_{2A} receptor binding affinity. These results were complemented by docking all these molecules to a very recent model of the 5-HT_{2B} receptor.

METHODS, MODELS AND CALCULATIONS

The formal method relating electronic structure with receptor binding affinity is now a standard one. The reader may consult references [24-29] if interested. The standard linear equation is:

$$pK_i = a + \sum_j \left[e_j Q_j + f_j S_j^E + s_j S_j^N \right] +$$
$$+ \sum_j \sum_m \left[h_j(m) F_j(m) + x_j(m) S_j^E(m) \right] + + \sum_j \sum_{m'} \left[r_j(m') F_j(m') + t_j(m') S_j^N(m') \right] +$$
$$+ \sum_j \left[g_j \mu_j + k_j \eta_j + o_j \omega_j + z_j \varsigma_j + w_j Q_j^{\max} \right] + \sum_{B=1}^{W} O_B \qquad (1)$$

where Q_i is the net charge of atom j, S_j^E and S_j^N are, respectively, the total atomic electrophilic and nucleophilic superdelocalizabilities of Fukui et al., $F_{j,m}$ ($F_{j,m'}$) is the Fukui index of the occupied (empty) MO m (m') located on atom j. $S_j^E(m)$ is the atomic electrophilic superdelocalizability of MO m on atom j, etc. The total atomic electrophilic superdelocalizability of atom j corresponds to the sum over occupied MOs of the $S_j^E(m)$'s and the total atomic nucleophilic superdelocalizability of atom j is the sum over empty MOs of the $S_j^N(m)$'s [30]. The last bracket of the right side of Eq. 1 contains a new set of local atomic reactivity indices obtained directly from the Hartree-Fock LCAO-MO and DFT models [25, 28, 29]. Below, $HOMO_j$* refers to the highest occupied molecular orbital localized on atom j and $LUMO_j$* to the lowest empty MO localized on atom j. μ_j is the local atomic electronic chemical potential of atom j (the $HOMO_j$*-$LUMO_j$* midpoint), η_j is the local atomic hardness of atom j (the $HOMO_j$*-$LUMO_j$* gap), ω_j is the local atomic electrophilicity of atom j, ς_j is the local atomic softness of atom j and $Q_j^{\max}$ is the maximal amount of electronic charge that atom j may accept from another site. The moment of inertia term of Eq. 1 can be expressed as:

$$\log\left[(ABC)^{-1/2} \right] = \sum_i \sum_t m_{i,t} R_{i,t}^2 = \sum_t O_t \qquad (2)$$

where the summation is over the different substituents of the molecule, $m_{i,t}$ is the mass of the i-th atom belonging to the t-th substituent, $R_{i,t}$ being its distance to the atom to which the substituent is attached. The physical interpretation of these terms is that they represent the portion of molecules attaining the correct orientation to interact with the receptor. We named them orientation parameters. The application of this method to the drug-receptor interaction has been very successful [13, 14, 16, 18, 19, 31-52]. The extension of

ISSN: 0975-8585

this method to any class of biological activities opened a completely new area of research [53-66]. The selected molecules are shown in Fig. 1 and Table 1.

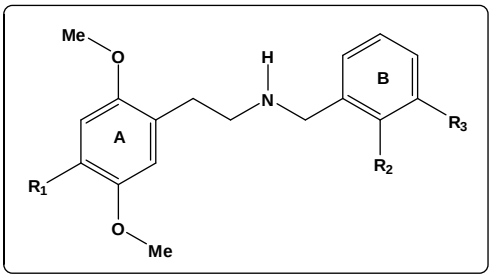

Figure 1: General formula of N-Benzylphenethylamines.

Table 1: Selected N-Benzylphenethylamines and their 5-HT_{2A} receptor binding affinity.

Mol.	Mol.	R_1	R_2	R_3	pK 5-HT_{2A}		Mol.	Mol.	R_1	R_2	R_3	pK 5-HT_{2A}
25	1	Br	OMe	H	9.3		227	23	Pr	F	H	8.51
26	2	Br	OH	H	9.47		228	24	Pr	O-CH_2-O		9.2
27	3	Br	F	H	8.57		229	25	SMe	OMe	H	9.27
28	4	Br	O-CH_2-O		9.22		230	26	SMe	OH	H	9.42
29	5	Cl	OMe	H	8.8		231	27	SMe	F	H	8.1
210	6	Cl	OH	H	9.21		232	28	SMe	O-CH_2-O		9.15
211	7	Cl	F	H	8.12		233	29	SEt	OMe	H	9.25
212	8	Cl	O-CH_2-O		9.00		234	30	SEt	OH	H	9.21
213	9	F	OMe	H	8.49		235	31	SEt	F	H	8.02
214	10	F	OH	H	8.34		236	32	SEt	O-CH_2-O		9.4
215	11	F	F	H	7.25		237	33	SPr	OMe	H	9.17
216	12	F	O-CH_2-O		7.92		238	34	SPr	OH	H	9.17
217	13	Me	OMe	H	8.7		239	35	SPr	F	H	8.6
218	14	Me	OH	H	8.96		240	36	SPr	O-CH_2-O		9.02
219	15	Me	F	H	7.72		241	37	CF_3	OMe	H	9.32
220	16	Me	O-CH_2-O		8.59		242	38	CF_3	OH	H	9.18
221	17	Et	OMe	H	9.48		243	39	CF_3	F	H	7.99
222	18	Et	OH	H	9.54		244	40	CF_3	O-CH_2-O		9
223	19	Et	F	H	8.63		245	41	CN	OMe	H	8.34
224	20	Et	O-CH_2-O		9.4		246	42	CN	OH	H	8.88
225	21	Pr	OMe	H	9.2		247	43	CN	F	H	7.2
226	22	Pr	OH	H	9.28		248	44	CN	O-CH_2-O		7.79

Molecule 41 was extracted from the set due to convergence problems during the geometry optimization procedure.

We carried out studies of three sets of molecules: the whole set (n=43, set I), a second set in which the R_1 substituent is an alkyl moiety (molecules 217-228 and 241-244, n=16, set II) and a third set in which R_1 is halogen, S-alkyl or CN (molecules 25-216, 229-240 and 246-248, n=27, set III). The common skeleton for all sets is shown in Fig. 2.

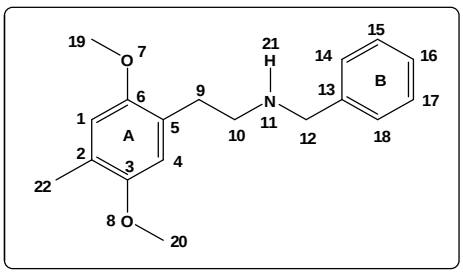

Figure 2: Numbering of the common skeleton.

ISSN: 0975-8585

We included in the common skeleton rings A and B, the heavy atoms of the linker joining them, one of the N protons, the oxygen and carbon atoms of both MeO substituents and the first atom attached to position 22 in Fig. 2. The biological activity selected is the ability of these compounds to displace [^{3}H]-ketanserin at 5-HT$_{2A}$ cloned human receptors. These data is expressed as pK and it is shown in Table 1. The electronic structure of all molecules was obtained within the DFT framework at the B3LYP/6-31g(d,p) level with full geometry optimization of the protonated form. The Gaussian suite of programs was used [67]. The numerical values of the LARIs were obtained with the D-CENT-QSAR software [68]. Mulliken Population Analysis results were corrected as usual [27]. Since it is not possible to solve the system of linear equations 1 due to the lack of sufficient molecules, we employed linear multiple regression analysis (LMRA) to find out the local atomic properties involved in the variation of the biological activity throughout the series. The Statistica software was used for LMRA [69]. We theorized that the variation of the values of one or more local atomic reactivity indices of a number of atoms belonging to the common skeleton above mentioned accounts for the variation of the binding affinity. One of the functions of the substituents is to modify the electronic structure of the common skeleton. We built a matrix containing the logarithm of the dependent variable (the pK's) and the local atomic reactivity indices of the atoms of the common skeleton as independent variables [28, 41]. Molecule 41 was not included in the set due to convergence problems during the geometry optimization procedure. For the 5-HT$_{2A}$ receptor, we used model 2 of the P28223 (Uniprot ID) structure generated by the GPCR-I-TASSER pipeline [70, 71]. Docking studies were carried out with Autodock Vina [72, 73]. LSD was docked with the rigid residue option. Subsequently, all the residues inside a 4 Å region around the ligand were considered to be flexible (they can change their conformation during the docking procedure). The lowest energy conformer of each study was selected for further analysis with Autodock Vina and Discovery Studio Visualizer [74]. Fig. 3 shows the binding site.

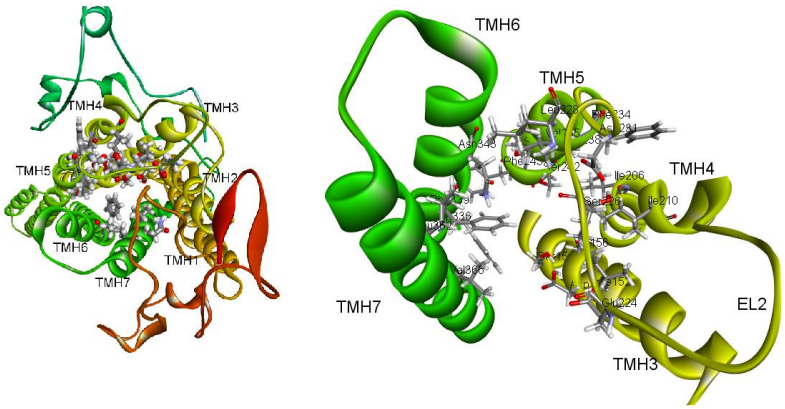

Figure 3. Left: 5HT$_{2A}$ receptor (the size of the flexible residues was enlarged for a better view). Right: closer view of the binding site. TMH refers to a transmembrane helix and EL to an extracellular loop (from [21]).

RESULTS

Results for the 5-HT$_{2A}$ binding affinity of the whole set of molecules (I)

For the original set (n=43), consecutive LMRA showed three outliers. They were extracted from the set and, for the remaining set (n=40), the best equation obtained was:

$$pK_i = 10.13 - 63.71\omega_{21} - 0.90S_3^E - 5.02S_{20}^E(HOMO)^* + 40.75F_{21}(HOMO)^* - \\ -0.03S_{21}^N(LUMO+2)^* \quad (3)$$

with n=40, R= 0.95, R²= 0.90, adjusted R²= 0.89, F(5,34)=63.05 (p<0.000001) and a standard error of estimate of 0.20. No outliers were detected and no residuals fall outside the ±2.00 σ limits. Here, ω_{21} is the local atomic electrophilicity of atom 21 (the NH proton), S_3^E is the total atomic electrophilic superdelocalizability of atom 3 (in ring A), $S_{20}^E(HOMO)^*$ is the orbital electrophilic superdelocalizability of

the highest occupied MO localized on atom 20 (the oxygen atom of a OMe substituent), $F_{21}(HOMO)^*$ is the Fukui index of the highest occupied MO localized on atom 21 (the NH proton) and $S_{21}^N(LUMO+2)^*$ is the orbital nucleophilic superdelocalizability of the third lowest vacant MO localized on atom 21 (the NH proton, see Fig. 2 for atom numbering). Tables 2 and 3 show, respectively, the beta coefficients, the results of the t-test for significance of coefficients and the matrix of squared correlation coefficients for the variables appearing in Eq. 3. Figure 4 shows the plot of observed *vs.* calculated values.

Table 2: Beta coefficients and t-test for significance of coefficients in Eq. 3.

	Beta	t(34)	p-level
ω_{21}	-0.55	-9.47	<0.000001
S_3^E	-0.68	-10.03	<0.000001
$S_{20}^E(HOMO)^*$	-0.39	-6.26	<0.000001
$F_{21}(HOMO)^*$	0.32	5.60	<0.000003
$S_{21}^N(LUMO+2)^*$	-0.15	-2.70	<0.01

Table 3: Matrix of squared correlation coefficients for the variables in Eq. 3.

	ω_{21}	S_3^E	$S_{20}^N(HOMO)^*$	$F_{21}(HOMO)^*$
S_3^E	0.06	1.00		
$S_{20}^N(HOMO)^*$	0.002	0.24	1.00	
$F_{21}(HOMO)^*$	0.04	0.04	0.004	1.00
$S_{21}^N(LUMO+2)^*$	0.02	0.005	0.004	0.03

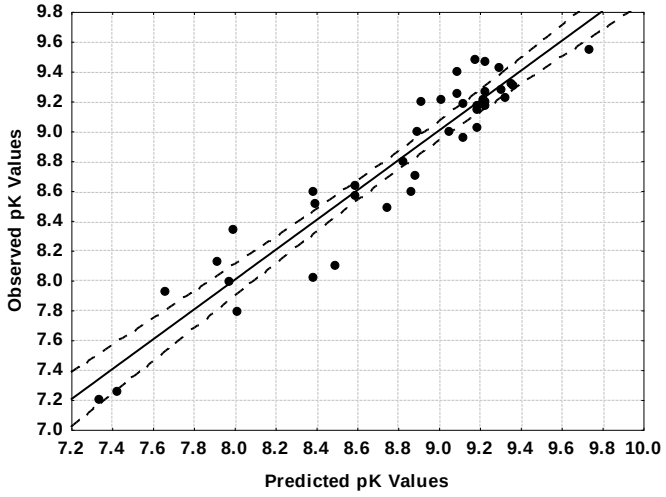

Figure 4: Plot of predicted *vs*. observed pK values (Eq. 3). Dashed lines denote the 95% confidence interval.

Table 3 shows that there are no significant internal correlations between independent variables. The associated statistical parameters of Eq. 3 show that this equation is statistically significant and that the simultaneous variation of a group of five local atomic reactivity indices belonging to the common skeleton explains about 89% of the variation of the 5-HT_{2A} receptor binding affinity. Figure 4, spanning about 2.5 orders of magnitude, shows that there is a good correlation of observed *versus* calculated values and that almost all

points are inside the 95% confidence interval. This can be considered as indirect evidence that the common skeleton hypothesis works relatively well. It is not possible to rule out the possibility that other atoms not belonging to the common skeleton directly interact with the receptors. These comments apply to all similar results presented below.

Results for the 5-HT$_{2A}$ binding affinity of set II

$$pK_i = 19.46 - 12.22Q_{21}^{max} - 1.06S_{15}^{E}(HOMO-2)^{*} + 7.31S_{10}^{E}(HOMO-1)^{*} \quad (4)$$

with n=15, R= 0.98, R²= 0.96, adjusted R²= 0.95, F(3,11)=91.35 (p<0.000001) and a standard error of estimate of 0.12. No outliers were detected and no residuals fall outside the ±2.00 σ limits. Here, Q_{21}^{max} is the maximal amount of charge atom 21 (the proton of NH) may receive, $S_{15}^{E}(HOMO-2)^{*}$ is the orbital electrophilic superdelocalizability of the third highest occupied MO localized on atom 15 (in ring B) and $S_{10}^{E}(HOMO-1)^{*}$ is the orbital electrophilic superdelocalizability of the second highest occupied MO localized on atom 10 (one of the carbon atoms of the NH-ring A linker). Tables 4 and 5 show, respectively, the beta coefficients, the results of the t-test for significance of coefficients and the matrix of squared correlation coefficients for the variables appearing in Eq. 4. Figure 5 shows the plot of observed *vs.* calculated values.

Table 4: Beta coefficients and t-test for significance of coefficients in Eq. 4.

	Beta	t(11)	p-level
Q_{21}^{max}	-0.72	-11.08	<0.000001
$S_{15}^{E}(HOMO-2)^{*}$	-0.60	-9.17	<0.000002
$S_{10}^{E}(HOMO-1)^{*}$	0.33	5.04	<0.0004

Table 5: Matrix of squared correlation coefficients for the variables in Eq. 4.

	Q_{21}^{max}	$S_{15}^{E}(HOMO-2)^{*}$
$S_{15}^{E}(HOMO-2)^{*}$	0.11	1.00
$S_{10}^{E}(HOMO-1)^{*}$	0.11	0.12

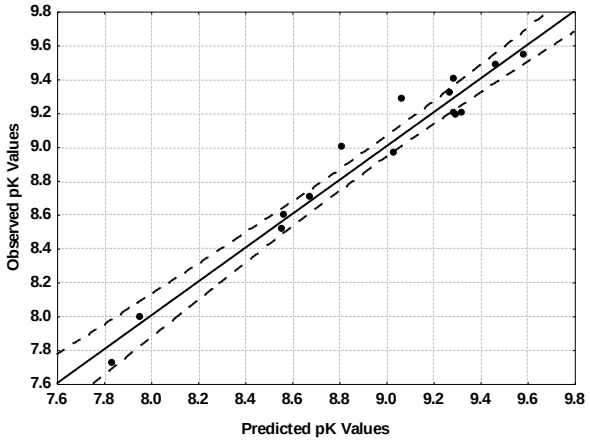

Figure 5: Plot of predicted *vs*. observed pK values (Eq. 4). Dashed lines denote the 95% confidence interval.

Table 5 shows that there are no significant internal correlations between independent variables. The associated statistical parameters of Eq. 4 show that this equation is statistically significant and that the

variation of a group of three local atomic reactivity indices belonging to the common skeleton explains about 96% of the variation of the 5-HT_{2A} receptor binding affinity. Figure 5, spanning about two orders of magnitude, shows that there is a good correlation of observed *versus* calculated values and that almost all points are inside the 95% confidence interval.

Results for the 5-HT_{2A} binding affinity of set III

$$pK_i = 15.18 - 0.61S_{22}^{E}(HOMO-1)^* - 17.83F_{17}(LUMO+1)^* + 25.72F_{13}(LUMO+1)^* - \\ -0.39S_{11}^{N}(LUMO+1)^* \quad (5)$$

with n=25, R= 0.97, R^2= 0.95, adjusted R^2= 0.94, F(4,20)=92.14 (p<0.000001) and a standard error of estimate of 0.16. No outliers were detected and no residuals fall outside the ±2.00 σ limits. Here, $S_{22}^{E}(HOMO-1)^*$ is the orbital electrophilic superdelocalizability of the second highest occupied MO localized on atom 22 (the atom directly bonded to the 2 position in ring A), $F_{17}(LUMO+1)^*$ is the Fukui index of the second lowest vacant MO localized on atom 17 (in ring B), $F_{13}(LUMO+1)^*$ is the Fukui index of the second lowest vacant MO localized on atom 13 (in ring B) and $S_{11}^{N}(LUMO+1)^*$ is the orbital nucleophilic superdelocalizability of the second lowest MO localized on atom 11 (the nitrogen atom). Tables 6 and 7 show, respectively, the beta coefficients, the results of the t-test for significance of coefficients and the matrix of squared correlation coefficients for the variables appearing in Eq. 5. Figure 6 shows the plot of observed *vs.* calculated values.

Table 6: Beta coefficients and t-test for significance of coefficients in Eq. 5.

	Beta	t(20)	p-level
$S_{22}^{E}(HOMO-1)^*$	-0.71	-13.63	<0.000001
$F_{17}(LUMO+1)^*$	-0.67	-11.21	<0.000001
$F_{13}(LUMO+1)^*$	0.28	4.95	<0.00008
$S_{11}^{N}(LUMO+1)^*$	-0.20	-3.37	<0.003

Table 7: Matrix of squared correlation coefficients for the variables in Eq. 5.

	$S_{22}^{E}(HOMO-1)^*$	$F_{17}(LUMO+1)^*$	$F_{13}(LUMO+1)^*$
$F_{17}(LUMO+1)^*$	0.05	1.00	
$F_{13}(LUMO+1)^*$	0.01	0.15	1.00
$S_{11}^{N}(LUMO+1)^*$	0.04	0.20	-0.13

Table 7 shows that there are no significant internal correlations between independent variables. The associated statistical parameters of Eq. 5 show that this equation is statistically significant and that the variation of a group of four local atomic reactivity indices belonging to the common skeleton explains about 94% of the variation of the 5-HT_{2A} receptor binding affinity. Figure 6, spanning about three orders of magnitude, shows that there is a good correlation of observed *versus* calculated values and that almost all points are inside the 95% confidence interval.

ISSN: 0975-8585

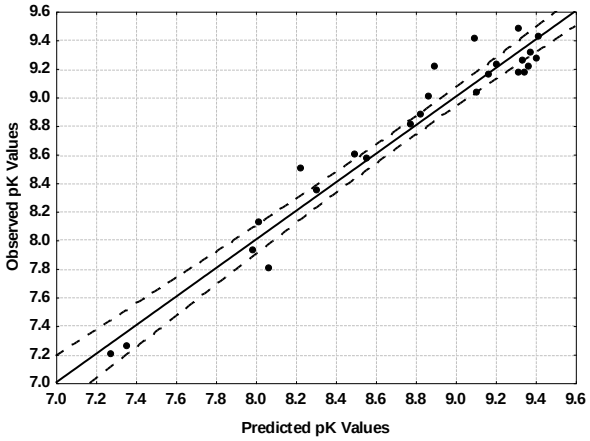

Figure 6: Plot of predicted *vs*. observed pK values (Eq. 5). Dashed lines denote the 95% confidence interval.

DOCKING RESULTS

Table 8 shows the color of the ligand-receptor interactions. A full discussion is presented below together with the corresponding figures.

Table 8: List of colors for docking figures analysis.

Interaction	Color name	RGB
Pi-alkyl (hydrophobic)	Cotton candy	(255,200,255)
Alkyl (hydrophobic)	Cotton candy	(255,200,255)
Pi-sigma (hydrophobic)	Heliotrope	(200,100,255)
Carbon-hydrogen bond	Honeydew	(220,255,220)
Conventional H-bond	Lime	(0,255,0)
Salt bridge (attractive charge)	Orange peel	(255,150,0)
Pi-anion	Orange peel	(255,150,0)
Pi-Pi stacked	Neon pink	(255,100,200)
Pi-Pi T shaped	Neon pink	(255,100,200)
Halogen	Aqua	(0,255,255)
Attractive charge	Orange peel	(255,150,0)
Carbon-hydrogen bond, halogen	Honeydew	(220,255,220)
Pi-sulphur	Tangerine yellow	(255,200,0)
Unfavorable donor-donor	Red	(255,10,0)
Unfavorable positive-positive	Red	(255,10,0)
Pi-cation	Orange peel	(255,150,0)
Unfavorable acceptor-acceptor	Red	(255,10,0)
Amide-π stacking	Neon pink	(255,100,200)

LOCAL MOLECULAR ORBITAL STRUCTURE

Tables 9 and 10 show the local molecular orbital structure of several atoms appearing in the QSAR equations (for other atoms see Ref. [23]).

Table 9: Local Molecular Orbital Structure of atoms 10, 11, 13 and 17.

Mol.	Atom 10 (C)	Atom 11 (N)	Atom 13 (C)	Atom 17 (C)
1 (98)	89σ93σ98σ- 99σ101σ102σ	82σ87σ94σ- 101σ105σ106σ	93π94π96π- 99π100π102π	93π94π96π- 99π100π101π
2 (94)	85σ90σ94σ- 95σ97σ98σ	82σ83σ89σ- 97σ101σ102σ	89π90π91π- 95π96π98π	89π90π91π- 95π96π101σ
3 (94)	85σ90σ94σ- 95σ97σ98σ	79σ80σ89σ- 97σ101σ102σ	83σ89π91π- 95π96π98π	89π90π91π- 95π96π101σ
4 (101)	87σ89σ90σ-	82σ83σ97σ-	91π97π99π-	91π97π99π-

	102σ105σ107σ	107σ108σ109σ	102π103π105π	102π103π105π
5 (89)	84σ88σ89σ-90σ92σ93σ	73σ78σ86σ-92σ95σ96	79π86π87π-90π91π93π	79π86π87π-90π91π92π
6 (85)	80σ84σ85σ-86σ87σ88σ	70σ73σ81σ-88σ91σ92σ	81π82π83π-86π87π89π	81π82π83π-86π87π89π
7 (85)	81σ84σ85σ-86σ88σ89σ	71σ72σ80σ-88σ91σ92σ	74σ80π83π-86π87π89π	80π81π83π-86π87π91π
8 (92)	77σ79σ81σ-93σ96σ99σ	73σ74σ89σ-98σ99σ100σ	83π89π91π-93π94π96π	82π89π91π-93π94π96π
9 (85)	81σ84σ85σ-86σ88σ89σ	71σ75σ82σ-88σ91σ92σ	77π82π83π-86π87π89π	77π82π83π-86π87π91π
10 (81)	77σ80σ81σ-82σ84σ85σ	68σ70σ78σ-84σ87σ88σ	77π78π79π-82π83π85π	77π78π79π-82π83π87σ
11 (81)	78σ80σ81σ-82σ85σ86σ	68σ69σ77σ-87σ88σ89σ	71σ77π79π-82π83π84π	77π78π79π-82π83π87σ
12 (88)	73σ76σ77σ-89σ91σ95σ	73σ77σ85σ-94σ95σ96σ	80π85π87π-89π90π91π	80π85π87π-89π90π91π
13 (85)	81σ84σ85σ-86σ88σ89σ	68σ74σ82σ-88σ91σ92σ	81π82π83π-86π87π89π	81π82π83π-86π87π91σ
14 (81)	78σ80σ81σ-82σ85σ89σ	69σ70σ77σ-87σ88σ89σ	77π78π79π-82π83π84π	77π78π79π-82π83π85π
15 (81)	78σ80σ81σ-82σ85σ88σ	67σ68σ77σ-87σ88σ89σ	70σ77π79π-82π83π84π	77π78π79π-82π83π87σ
16 (88)	76σ77σ80σ-89σ91σ95σ	70σ76σ85σ-94σ95σ96σ	84π85π86π-89π90π91π	79π85π86π-89π90π91π
17 (89)	86σ88σ89σ-90σ92σ93σ	71σ72σ76σ-92σ95σ96σ	85π86π87π-90π91π93π	85π86π87π-90π91π95σ
18 (85)	68σ69σ75σ-87σ90σ93σ	61σ63σ66σ-90σ91σ93σ	81π82π83π-86π88π90σ	81π82π83π-86π88π89π
19 (85)	82σ84σ85σ-86σ89σ92σ	69σ70σ81σ-91σ92σ93σ	72π81π83π-86π87π88π	81π82π83π-86π87π91σ
20 (92)	77σ78σ80σ-93σ95σ99σ	72σ75σ78σ-98σ99σ100σ	88π89π90π-93π94π95π	88π89π90π-93π94π95π
21 (93)	90σ92σ93σ-94σ96σ97σ	73σ79σ89σ-96σ99σ100σ	89π90π91π-94π95π97π	89π90π91π-94π95π99σ
22 (89)	86σ88σ89σ-90σ93σ97σ	74σ75σ85σ-95σ96σ97σ	75π85π87π-90π91π93π	75π85π87π-90π91π93π
23 (89)	87σ88σ89σ-90σ93σ96σ	70σ72σ85σ-95σ96σ97σ	85π86π87π-90π91π92π	85π86π87π-90π91π92π
24 (96)	81σ82σ83σ-97σ99σ103σ	74σ75σ92σ-102σ103σ104σ	92π93π94π-97π98π99π	84π92π94π-97π98π99π
25 (93)	88σ91σ93σ-94σ96σ97σ	75σ81σ89σ-96σ99σ100σ	88π89π90π-94π95π97π	88π89π90π-94π95π99π
26 (89)	85σ87σ89σ-90σ92σ93σ	76σ77σ84σ-92σ95σ96σ	84π85π86π-90π91π93π	84π85π86π-90π91π93π
27 (89)	85σ87σ89σ-90σ92σ93σ	72σ73σ84σ-92σ95σ96σ	83π84π86π-90π91π93π	84π85π86π-90π91π95π
28 (96)	79σ84σ85σ-97σ100σ103σ	75σ76σ92σ-102σ103σ104σ	86π92π94π-97π98π100π	86π92π94π-97π98π100π
29 (97)	93σ95σ97σ-98σ100σ101σ	77σ78σ83σ-100σ103σ104σ	92π93π94π-98π99π101π	92π93π94π-98π99π103π
30 (93)	89σ91σ93σ-94σ96σ97σ	78σ79σ88σ-96σ99σ100σ	88π89π90π-94π95π97π	88π89π90π-94π95π97π
31 (93)	89σ91σ93σ-94σ96σ97σ	75σ76σ77σ-96σ99σ100σ	88π89π90π-94π95π97π	88π89π90π-94π95π99π
32 (100)	83σ85σ86σ-101σ104σ107σ	78σ79σ96σ-106σ107σ108σ	95π96π98π-101π102π104π	95π96π98π-101π102π104π
33 (101)	97σ99σ101σ-102σ104σ105σ	79σ86σ96σ-104σ107σ108σ	96π97π98π-102π103π105π	96π97π98π-102π103π107σ
34 (97)	93σ95σ97σ-98σ100σ101σ	80σ82σ92σ-100σ103σ104σ	82π92π94π-98π99π101π	92π93π94π-98π99π101π
35 (97)	93σ95σ97σ-	76σ78σ91σ-	91π93π94π-	92π93π94π-

	98σ100σ101σ	100σ103σ104σ	98π99π101π	98π99π103π
36 (104)	99σ101σ104σ-105σ107σ108σ	80σ81σ100σ-106107110	99π100π102π-105π106π108π	91π100π102π-105π106π107π
37 (97)	84σ85σ95σ-98σ99σ101σ	80σ87σ93σ-99σ103σ104σ	89π93π96π-98π100π101π	93π95π96π-98π99π100π
38 (93)	83σ89σ92σ-94σ96σ97σ	78σ83σ90σ-96σ99σ100σ	90π91π92π-94π95π97π	90π91π92π-94π95π96π
39 (93)	79σ83σ92σ-94σ96σ97σ	75σ77σ78σ-96σ99σ100σ	89π90π91π-94π95π97π	89π90π91π-94π95π99π
40 (100)	81σ83σ88σ-101σ104σ107σ	80σ81σ97σ-106σ107σ108σ	92π97π99π-101π102π104π	92π97π99π-101π102π104π
42 (83	73σ79σ82σ-84σ85σ87σ	71σ72σ80σ-89σ90σ91σ	72π80π81π-84π85π86π	72π80π81π-84π86π89π
43 (83)	73σ79σ82σ-84σ85σ87σ	68σ70σ80σ-85σ89σ90σ	79π80π81π-84π86π87π	79π80π81π-84π86π91π
44 (90)	76σ77σ78σ-91σ94σ97σ	72σ78σ87σ-96σ97σ98σ	80π87π89π-91π93π94π	80π87π89π-91π93π94π

Table 10: Local Molecular Orbital Structure of atoms 21 and 22.

Mol.	Atom 21 (H)	Atom 22 (X)
1 (98)	71σ74σ78σ-99σ100σ101σ	96lp97π98π-101lp104σ105σ
2 (94)	71σ73σ76σ-95σ96σ97σ	92lp93π94π-97lp100σ101σ
3 (94)	69σ73σ76σ-95σ96σ97σ	92lp93π94π-97lp100σ101σ
4 (101)	71σ72σ81σ-102σ104σ105σ	98lp100π101π-104π106σ107σ
5 (89)	60σ62σ65σ-90σ91σ92σ	86lp88π89π-92lp95σ96σ
6 (85)	56σ58σ66σ-86σ87σ89σ	82lp84π85π-88lp92σ93σ
7 (85)	54σ59σ60σ-86σ87σ88σ	82lp84π85π-88lp91σ92σ
8 (92)	62σ63σ72σ-93σ95σ96σ	88lp90π92π-95lp99σ101σ
9 (85)	49σ57σ59σ-86σ87σ88σ	81π84lp85lp-88lp94σ97σ
10 (81)	54σ59σ63σ-82σ83σ84σ	77π80π81π-84lp91σ93σ
11 (81)	53σ56σ57σ-82σ83σ84σ	78lp80lp81lp-84lp85lp92σ
12 (88)	57σ58σ60σ-89σ91σ92σ	84π86lp88lp-92lp93lp101σ
13 (85)	57σ58σ65σ-86σ87σ88σ	79σ80σ84σ-98σ106σ110σ
14 (81)	56σ60σ63σ-82σ83σ84σ	75σ76σ80σ-94σ103σ106σ
15 (81)	55σ60σ63σ-82σ83σ84σ	75σ76σ80σ-93σ102σ104σ
16 (88)	55σ58σ59σ-89σ91σ92σ	82σ83σ87σ-102σ104σ109σ
17 (89)	58σ59σ60σ-90σ91σ92σ	84σ86σ88σ-92σ102σ110σ
18 (85)	52σ54σ63σ-86σ87σ88σ	81σ84σ85σ-89σ97σ104σ
19 (85)	51σ57σ62σ-86σ87σ88σ	80σ82σ84σ-97σ105σ109σ
20 (92)	55σ60σ61σ-93σ95σ96σ	86σ87σ91σ-96σ106σ113σ
21 (93)	60σ61σ62σ-94σ95σ96σ	88σ90σ92σ-96σ106σ114σ
22 (89)	57σ60σ64σ-90σ91σ92σ	84σ86σ88σ-102σ108σ109σ
23 (89)	53σ59σ64σ-90σ91σ92σ	86σ87σ88σ-101σ109σ113σ
24 (96)	57σ62σ63σ-97σ99σ100σ	91σ93σ95σ-100σ117σ120σ
25 (93)	63σ64σ67σ-94σ95σ96σ	91lp92π93π-96lp98lp99lp
26 (89)	59σ64σ66σ-90σ91σ92σ	87lp88lp89lp-92lp94lp96lp
27 (89)	55σ61σ66σ-90σ91σ92σ	87lp88lp89lp-92lp94lp97σ
28 (96)	64σ65σ74σ-97σ100σ102σ	93lp95π96π-99lp101lp104σ
29 (97)	65σ66σ69σ-98σ99σ100σ	95lp96π97π-100lp102lp103lp
30 (93)	61σ66σ68σ-94σ95σ96σ	91lp92lp93lp-96lp98lp100σ
31 (93)	57σ63σ68σ-94σ95σ96σ	91lp92lp93lp-96lp98lp101σ
32 (100)	61σ66σ67σ-101σ104σ106σ	97lp99lp100lp-103lp105lp108σ
33 (101)	68σ71σ77σ-102σ103σ104σ	99lp100lp101lp-104lp106lp109σ
34 (97)	61σ63σ70σ-98σ99σ100σ	95lp96lp97lp-100lp102lp104lp
35 (97)	59σ65σ70σ-98σ99σ100σ	95lp96lp97lp-100lp102lp104lp
36 (104)	68σ69σ74σ-105σ107σ108σ	101lp103lp104lp-107lp109lp112σ
37 (97)	60σ65σ67σ-98σ99σ100σ	88σ90σ91σ-99π110σ112π
38 (93)	62σ67σ69σ-94σ95σ97σ	84σ87σ88σ-96π98π105σ
39 (93)	64σ65σ69σ-94σ95σ96σ	84σ87σ88σ-96π98π105σ
40 (100)	67σ68σ77σ-101σ103σ104σ	94σ95σ98π-103π105π115σ

42 (83)	60σ62σ65σ-84σ85σ86σ	79π82π83π-85π88π90π
43 (83)	54σ58σ65σ-84σ85σ86σ	79π82π83π-85π88π90π
44 (90)	59σ61σ70σ-91σ94σ96σ	86π88π90π-92π95π98π

DISCUSSION

To interpret the results we must consider that it is the *simultaneous* variation of the numerical values of the LARIs appearing in the equations which explains the variation of the activity through the group. Also, all molecular orbital-related LARIs employed here (Fukui indices and orbital superdelocalizabilities) have non-zero values (this is so because of the way we build the data matrix). Then, it is of common sense to accept that if, for example, an occupied MO different from the HOMO and localized on a particular atom appears in the equations, the occupied MOs having a lower energy and localized on the same atom also participate in the interaction (the same reasoning holds for vacant MOs). We carried out the analysis by employing the *variable-by-variable* (VbV) approach: the conditions that a reactivity index must fulfill for a high pK_i are determined and the corresponding interaction or interactions are proposed. In the case of the orbital-related LARIs the nature (σ, π and lone pair) of the MOs must be taken into account.

Discussion of the 5-HT_{2A} binding results

Discussion of the 5-HT_{2A} binding affinity results for the whole set (I)

The beta values (Table 2) show that the relative importance of the reactivity indices is S_3^E > ω_{21} > $S_{20}^E(HOMO)^*$ > $F_{21}(HOMO)^*$ >> $S_{21}^N(LUMO+2)^*$.

A variable-by-variable analysis indicates that a high pK value is associated with a small numerical value for ω_{21} and with high numerical values for $|S_3^E|$, $|S_{20}^E(HOMO)^*|$ and $F_{21}(HOMO)^*$. If $S_{21}^N(LUMO+2)^*$ values are positive a small value is required; if negative a high value of $|S_{21}^N(LUMO+2)^*|$ is needed. Because of the results of the Student t-test $S_{21}^N(LUMO+2)^*$ will not be discussed. There are two local atomic reactivity indices involving one of the hydrogen atoms (atom 21) attached to the nitrogen atom (see Fig.2). Let us first consider the condition of a small value for ω_{21}. We have defined the local atomic electrophilicity of atom i as [29]:

$$\omega_i = \mu_i^2 / 2\eta_i \qquad (6)$$

where μ_i is the local atomic electronic chemical potential of atom i (the $HOMO_i^*$-$LUMO_i^*$ midpoint) and η_i is the local atomic hardness of atom i (the $HOMO_i^*$-$LUMO_i^*$ gap). The ideal procedure to get a small value for ω_i, combining the physical meanings of μ_i and η_i, is by approaching the $HOMO_i^*$-$LUMO_i^*$ midpoint to zero in the energy axis and simultaneously increasing the $HOMO_i^*$-$LUMO_i^*$ gap. Considering now that in general μ_i values are negative this can be done by moving upwards the LUMO energy and therefore diminishing the tendency of atom i to receive electrons. Then, atom 21 should have a low propensity to receive electrons. A high numerical value for $F_{21}(HOMO)^*$, a σ MO, suggests that a high pK value is associated with a high σ electron population on this atom/MO (see Table 10). This, in turn, strongly suggests that atom 21 is possibly interacting with a center having vacant MOs. A highly negative value for S_3^E indicates that atom 3, a carbon atom of ring A, is interacting with an electron-deficient center. A high negative value for $S_{20}^E(HOMO)^*$ is required. Atom 20 is the carbon atom of one of the OMe substituents in ring A (see Fig. 2). $(HOMO)_{20}^*$ is a σ MO [23]. Then, atom 20 seems to be involved in an attractive interaction in with an empty MO. These ideas are summarized in the partial two dimensional (2D) pharmacophore shown in Fig. 7.

ISSN: 0975-8585

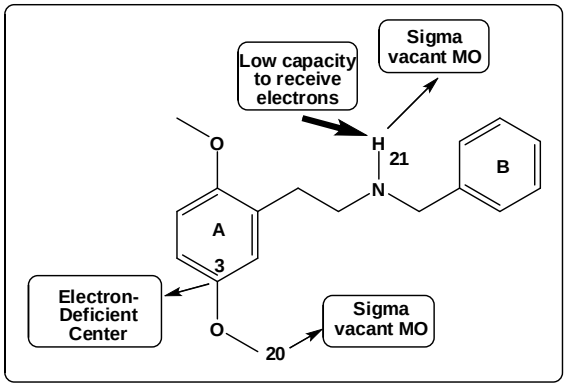

Figure 7: Partial 2D pharmacophore for the interaction of group I of molecules with the 5-HT$_{2A}$ receptor.

Discussion of the 5-HT$_{2A}$ binding affinity results for set II

The beta values (Table 4) show that the relative importance of the reactivity indices is $Q_{21}^{\max}$ > $S_{15}^{E}(HOMO-2)^{*}$ > $S_{10}^{E}(HOMO-1)^{*}$.

A VbV analysis indicates that a high pK value is associated with small value for $Q_{21}^{\max}$ (a positive variable), with high negative values for $S_{15}^{E}(HOMO-2)^{*}$ and with small negative numerical values for $S_{10}^{E}(HOMO-1)^{*}$. Here we have LARIs belonging to the N proton, a carbon atom of ring B and one of the carbon atoms of the linker joining ring A and NH moieties. A small value for $Q_{21}^{\max}$ is indicative of a low capacity to receive electrons, fact that is in perfect agreement with the results for the whole set (set I). A high negative value for $S_{15}^{E}(HOMO-2)^{*}$, a σ or π MO, suggests that atom 15 is interacting with an electron-deficient center through its three highest occupied local MOs ($(HOMO-1)_{15}^{*}$ is a σ or π MO and $(HOMO)_{15}^{*}$ is a π MO). A small numerical value for $S_{10}^{E}(HOMO-1)^{*}$ (a CH_2 carbon atom with only σ MOs) suggests that only $(HOMO)_{10}^{*}$ is interacting with a moiety with vacant σ MOs. The partial 2D pharmacophore containing these suggestions is shown in Fig. 8.

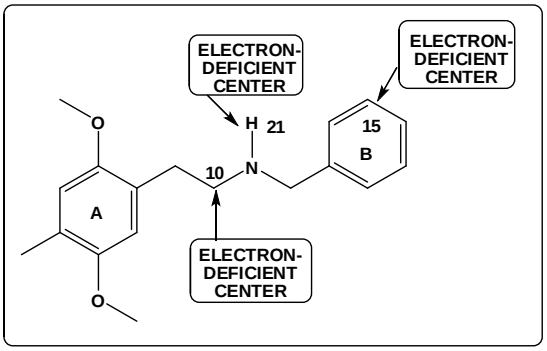

Figure 8: Partial 2D pharmacophore for the interaction of group II of molecules with the 5-HT$_{2A}$ receptor.

Discussion of the 5-HT$_{2A}$ binding affinity results for set III

The beta values (Table 6) show that the relative importance of the reactivity indices is $S_{22}^{E}(HOMO-1)^{*}$ > $F_{17}(LUMO+1)^{*}$ >> $F_{13}(LUMO+1)^{*}$ > $S_{11}^{N}(LUMO+1)^{*}$. Here we have LARIs of the atom directly bonded to carbon 2 in ring A, of two carbon atoms belonging to ring B (atoms 13 and 17) and of the N atom. A variable-by-variable analysis indicates that a high pK value is associated with small

positive values for $F_{17}(LUMO+1)^*$, with high values for $F_{13}(LUMO+1)^*$ and with highly negative values for $S_{22}^{E}(HOMO-1)^*$. In the case of $S_{11}^{N}(LUMO+1)^*$, if the numerical values are positive small ones are associated with high pK values. If they are negative, high pK values are associated with high values of $\left|S_{11}^{N}(LUMO+1)^*\right|$. $(LUMO+1)_{17}^{*}$ is a π MO (Table 9). A low value for $F_{17}(LUMO+1)^*$ suggests that $(LUMO)_{17}^{*}$ could be interacting with an electron-rich moiety and that probably $(LUMO+1)_{17}^{*}$ has an unfavorable interaction with vacant MOs of the binding site [75, 76]. $(LUMO+1)_{13}^{*}$ is a π MO (Table 9). A high value for $F_{13}(LUMO+1)^*$ indicates that atom 13 is interacting with an electron-rich center through its first two lowest vacant MOs. Atom 11 is the nitrogen atom in the chain connecting rings A and B (Fig. 2). All MOs are of σ nature (Table 9). The condition imposed by Eq. 5 to $S_{11}^{N}(LUMO+1)^*$ requires that the vacant MO energies move upwards in the energy axis. This suggests that atom 11 should act as an electron-donor center. Atom 22 is first atom of the substituent at position 4 connected to ring A and it seems to be very important for the psychoactive effects of 2,5-dimethoxy-4-X-phenylethylamines and 2,5-dimethoxy-4-X-amphetamines. Table 10 shows that the electronic structure of this atom is strongly dependent of the kind of substituent. It is important to stress that this is the first time that a LARI associated to this substituent appears in a model-based method [77]. A high value for $S_{22}^{E}(HOMO-1)^*$ is required for high receptor binding affinity. Considering that $(HOMO-1)_{22}^{*}$ can be a π, σ or lone pair MO, we may only suggest the possible participation of this atom in interaction(s) with an electron-deficient center. The corresponding partial 2D pharmacophore is shown in Fig. 9.

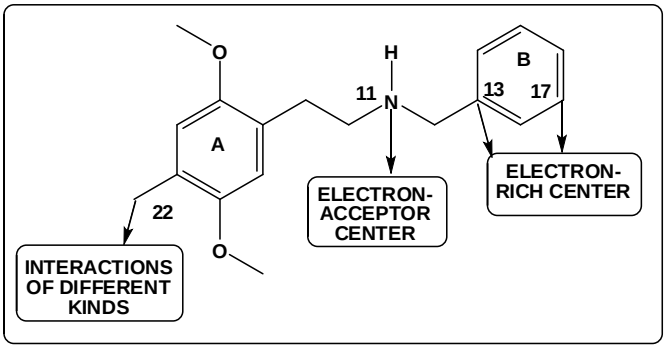

Figure 9: Partial 2D pharmacophore for the interaction of group III of molecules with the 5-HT$_{2A}$ receptor.

If we combine Fig. 7 to 9 we obtain the final 2D partial pharmacophore shown in Fig. 10. Note that there are no incompatibilities between the different suggestions.

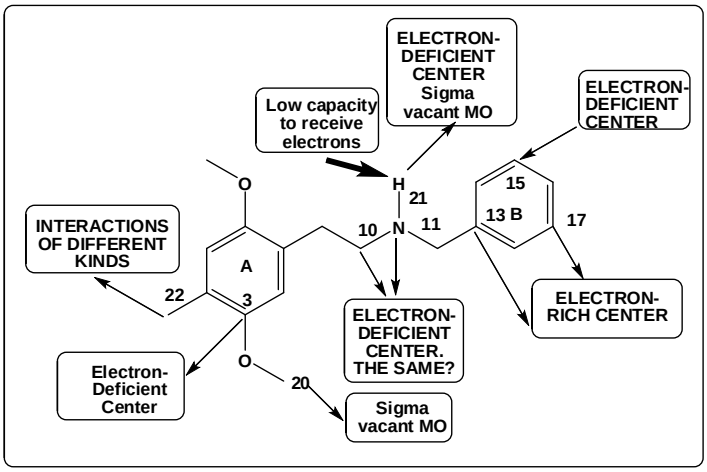

Figure 10: Partial final 2D pharmacophore for the binding of N-Benzylphenethylamines to the 5-HT$_{2A}$ receptor.

ISSN: 0975-8585

DOCKING

The docking results are presented below for the 44 molecules together with a list of detected interactions.

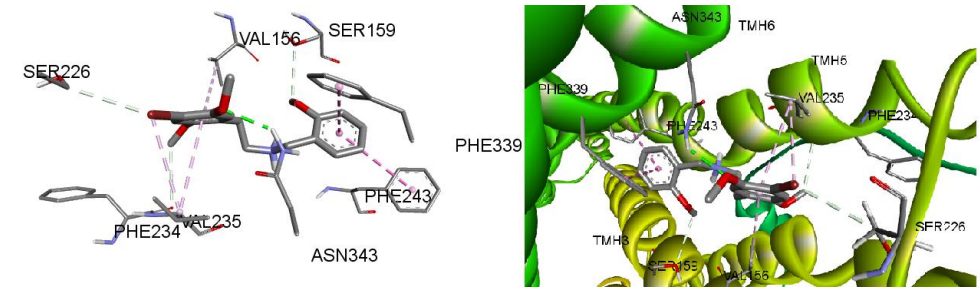

Figure 11: Molecule 1 docked to the 5-HT$_{2A}$ binding site.

We can observe the following interactions (see Fig. 2 for atom numbering): π-alkyl interactions of ring A with Val-156 (5.28Å) and Val-235 (4.81Å), an alkyl interaction of Br with Val-235 (4.41Å), a carbon H-bond between Br and Ser-226 (3.68Å), a carbon H-bond between C19 and the backbone of Phe-234 (3.43Å), a conventional H-bond between O8 and Asn-343 (2.29Å), a π-π T-shaped interaction of ring B with Phe-339 (4.91Å), a π-π stacking interaction of ring B with Phe-243 (5.58Å) and carbon H-bonds between the Me part of the 2-OMe substituent in ring B and Ser-159 (3.31Å).

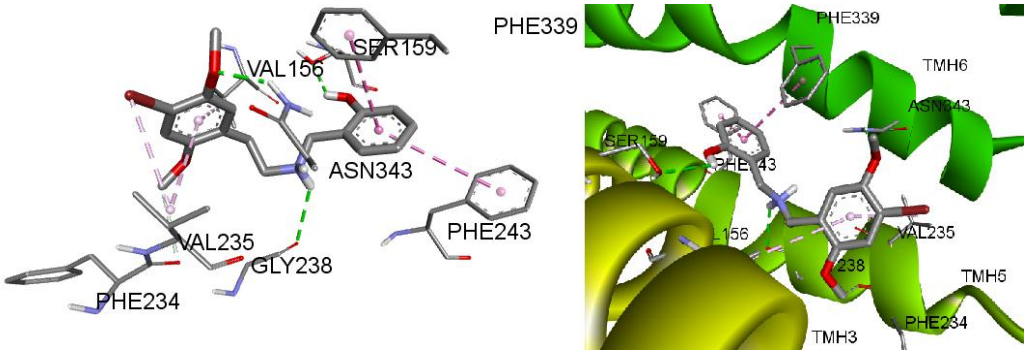

Figure 12: Molecule 2 docked to the 5-HT$_{2A}$ binding site.

Here we observe the following interactions: π-alkyl interactions of ring A with Val-156 (5.38Å) and Val-235 (4.76Å), an alkyl interaction of Br with Val-235 (4.33Å), a carbon H-bond between C19 and the backbone of Phe-234 (3.42Å), a conventional H-bond between O8 and Asn-343 (2.25Å), a π-π T-shaped interaction of ring B with Phe-339 (4.81Å), a π-π stacking interaction of ring B with Phe-243 (5.58Å), a conventional H-bond between the hydrogen atom of the 2-OH substituent in ring B and Ser-159 (2.75Å) and a conventional H-bond between H21 and the backbone of Gly-238 (2.88Å).

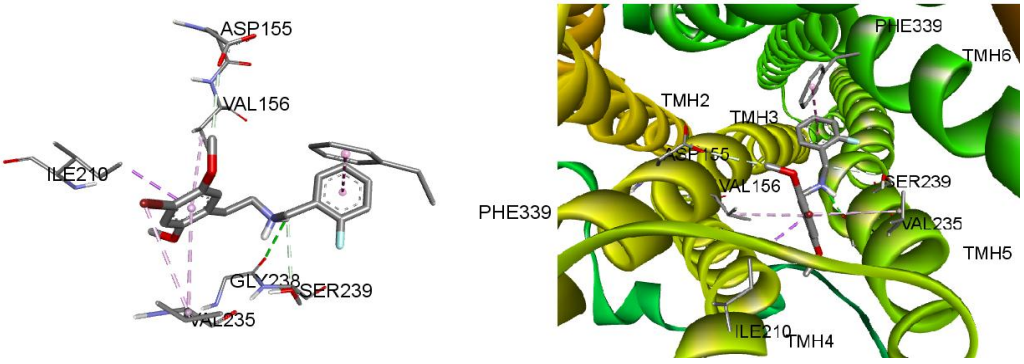

Figure 13: Molecule 3 docked to the 5-HT$_{2A}$ binding site.

ISSN: 0975-8585

Here we can see the following interactions: π-alkyl interactions of ring A with Val-156 (4.59Å) and Val-235 (5.21Å), a π-σ interaction of ring A with Ile-210 (3.98Å), an alkyl interaction of Br with Val-235 (4.73Å), a carbon H-bond between C20 and Asp-155 (3.68Å), a π-π T-shaped interaction of ring B with Phe-339 (4.92Å), a carbon H-bond between C12 and Ser-239 (3.62Å) and a conventional H-bond between H21 and the backbone of Gly-238 (3.01Å).

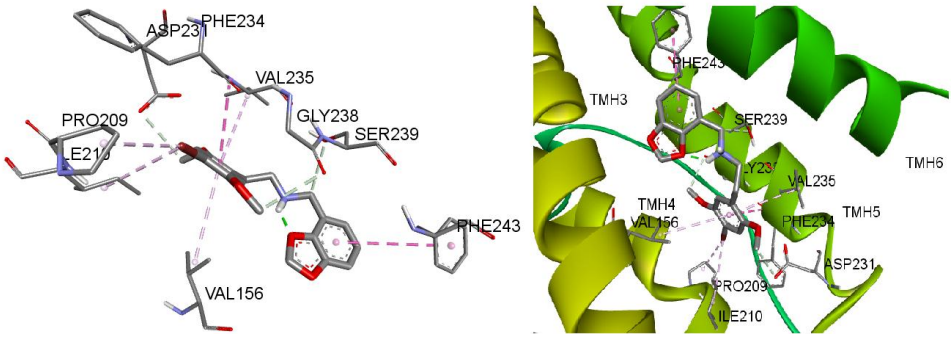

Figure 14: Molecule 4 docked to the 5-HT$_{2A}$ binding site.

The following interactions appear (see Fig. 2): π-alkyl interactions of ring A with Val-156 (4.77Å) and Val-235 (5.20Å), amide-π stacking interactions of ring A with the backbone of Phe-234 and Val-235 (4.18Å), alkyl interactions of Br with Pro-209 (4.35Å) and Ile-210 (4.82Å), a carbon H-bond between C19 and Asp-231 (3.59Å), a carbon H-bond between C20 and the backbone of Gly-238 (3.32Å), a π-π stacking interaction of ring B with Phe-243 (5.86Å) and a carbon H-bond between C12 and Ser-239 (3.25Å). There is an intramolecular H-bond between H21 and the oxygen atom of the methylenedioxy substituent (1.94Å).

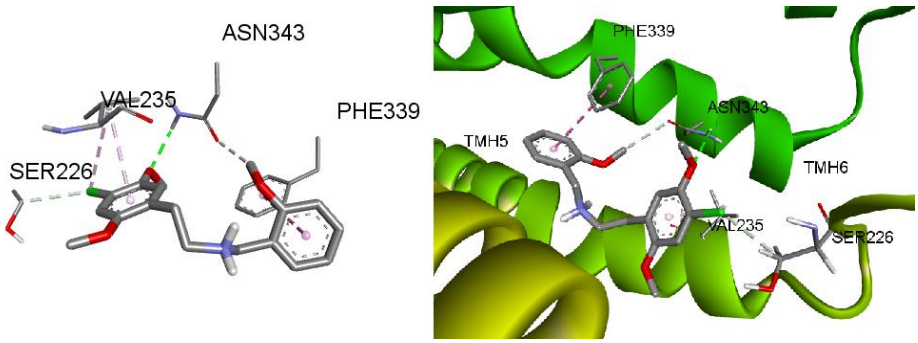

Figure 15: Molecule 5 docked to the 5-HT$_{2A}$ binding site.

The following interactions are observed: a π-alkyl interaction of ring A with Val-235 (4.00Å), an alkyl interaction of Cl with Val-235 (4.64Å), a carbon H-bond between Cl and Ser-226 (3.52Å), a conventional H-bond between O8 and Asn-343 (2.46Å), a π-π T- shaped interaction of ring B with Phe-339 (4.96Å) and a carbon H-bond between the Me part of the 2-OMe substituent in ring B and Asn-343 (3.22Å).

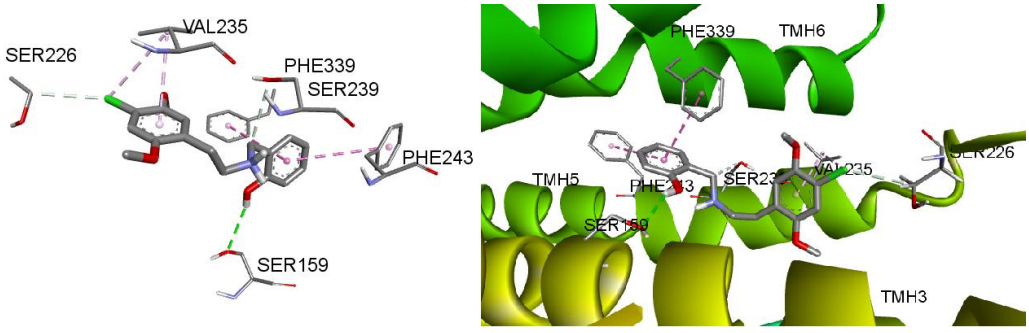

Figure 16: Molecule 6 docked to the 5-HT$_{2A}$ binding site.

ISSN: 0975-8585

In this case we can observe the following interactions: a π-alkyl interaction of ring A with Val-235 (4.28Å), an alkyl interaction of Cl with Val-235 (4.52Å), a carbon H-bond between Cl and Ser-226 (3.54Å), a π-π T-shaped interaction of ring B with Phe-339 (4.88Å), a π-π stacking interaction of ring B with Phe-243 (5.66Å), a conventional H-bond between the hydrogen atom of the 2-OH substituent in ring B and Ser-159 (2.87Å) and a carbon H-bond between C12 and Ser-239 (3.59Å).

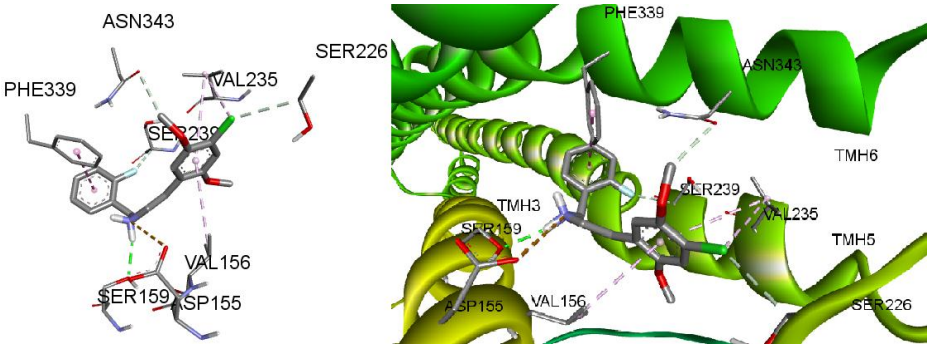

Figure 17: Molecule 7 docked to the 5-HT$_{2A}$ binding site.

The following interactions are observed: π-alkyl interactions of ring A with Val-156 (4.76Å) and Val-235 (5.39Å), an alkyl interaction of Cl with Val-235 (4.56Å), a carbon H-bond between Cl and Ser-226 (3.68Å), a carbon H-bond between C20 and Asn-343 (3.55Å), a π-π T-shaped interaction of ring B with Phe-339 (4.82Å), a carbon H-bond between F in ring B and Ser-239 (3.50Å), an attractive charge interaction of N11 and Asp-155 (5.26Å) and a conventional H-bond between H21 and Ser-159 (2.15Å).

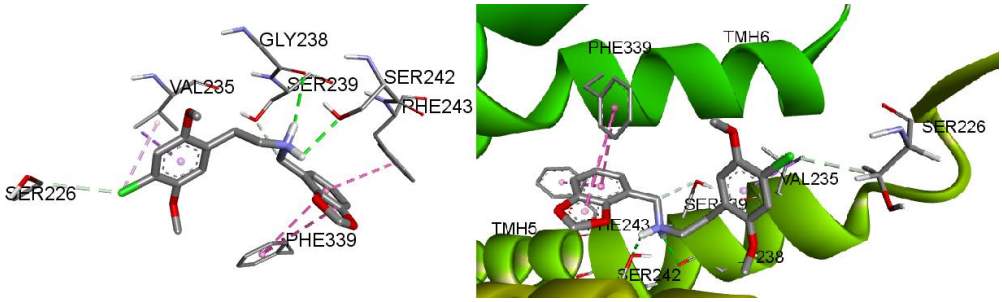

Figure 18: Molecule 8 docked to the 5-HT$_{2A}$ binding site.

Here we observe the following interactions: a π-σ interaction of ring A with Val-235 (3.89Å), an alkyl interaction of Cl with Val-235 (4.80Å), a carbon H-bond between Cl and Ser-226 (3.60Å), a π-π T-shaped interaction of ring B with Phe-339 (4.79Å), a π-π stacking interaction of ring B with Phe-243 (5.53Å), a π-π T-shaped interaction of the methylenedioxy moiety and Phe-339 (5.20Å), a conventional H-bond between one hydrogen from the amine moiety and Ser-242 (2.54Å), a conventional H-bond between H21 and Gly-238 (2.48Å) and a carbon H-bond between C12 and Ser-239 (3.21Å).

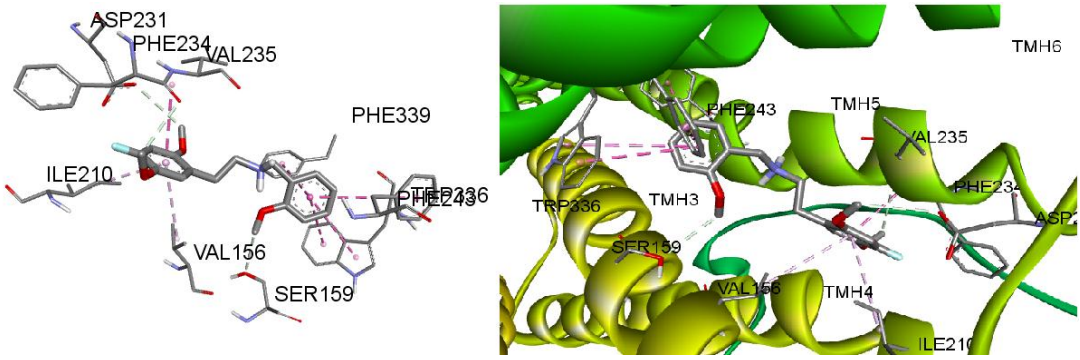

Figure 19: Molecule 9 docked to the 5-HT$_{2A}$ binding site.

ISSN: 0975-8585

In this case the following interactions are observed: π-alkyl interactions of ring A with Val-156 (4.83Å) and Ile-210 (5.12Å), amide-π interactions of ring A with the backbone of Phe-234 and Val-235 (3.98Å), a carbon H bond between C20 and the backbone of Phe-234 (3.50Å),a carbon H-bond between C19 and Asp-231 (3.60Å), a π-π T-shaped interaction of ring B with Phe-339 (4.85Å), π-π stacking interactions of ring B with two rings of Trp-336 (5.66Å and 5.04Å) and Phe-243 (5.72Å), and a conventional H-bond between the Me part of the 2-OMe substituent in ring B and Ser-159 (3.32Å).

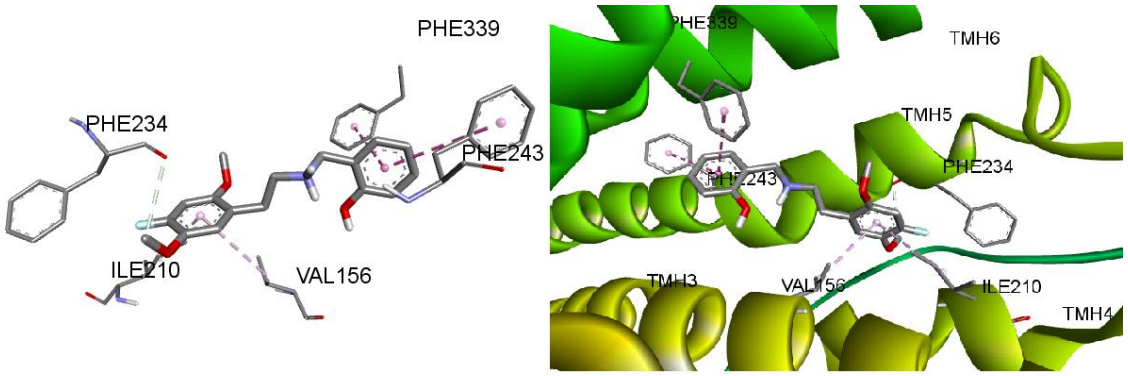

Figure 20: Molecule 10 docked to the 5-HT$_{2A}$ binding site.

Here we can observe π-alkyl interactions of ring A with Val-156 (4.78Å) and Ile-210 (5.11Å), a carbon H-bond between C20 and Phe-234 (3.43Å), a π-π T-shaped interaction of ring B with Phe-339 (4.90Å) and a π-π stacking interaction of ring B with Phe-243 (5.69Å).

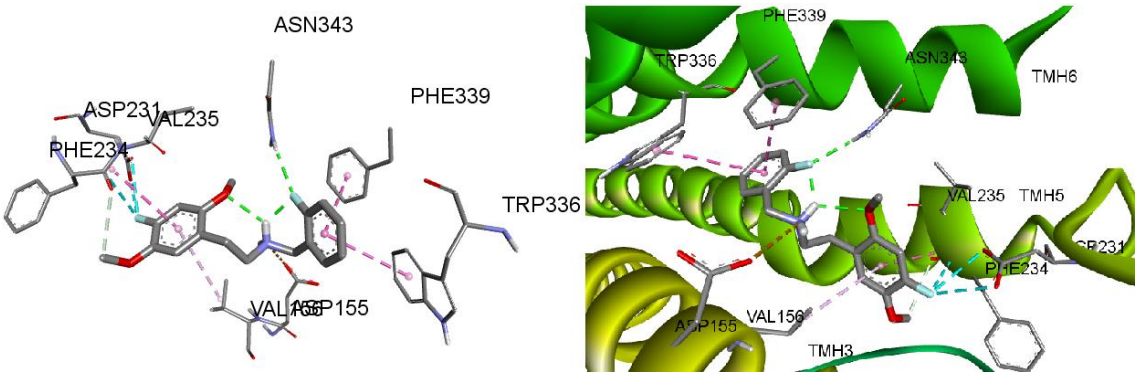

Figure 21: Molecule 11 docked to the 5-HT$_{2A}$ binding site.

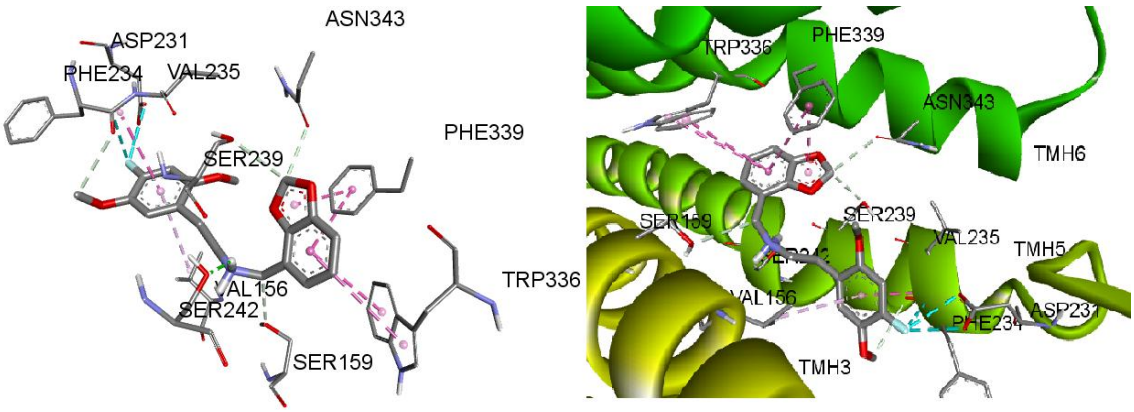

Figure 22: Molecule 12 docked to the 5-HT$_{2A}$ binding site.

Here we can observe a π-alkyl interaction of ring A with Val-156 (4.65Å), amide-π interactions of ring A with the backbone of Phe-234 and Val-235 (4.18Å), a carbon H-bond between C20 and the backbone of Phe-234 (3.34Å), halogen interactions of the fluorine in ring A with the backbone of Phe-234 (3.59Å) and the two oxygen atoms in Asp-231 (3.20Å and 3.37Å), π-π stacking interactions of ring B with Phe-339 (4.50Å) and Trp-336 (4.72Å), a conventional H-bond between F in ring B and Asn-343 (2.36Å) and an attractive charge interaction of N11 and Asp-155 (5.26Å). There are intramolecular H-bonds between H21 with F in ring B (1.99Å) and with O7 (2.46Å).

Here we can observe a π-alkyl interaction of ring A with Val-156 (4.65Å), amide-π interactions of ring A with the backbone of Phe-234 and Val-235 (4.09Å), a carbon H-bond between C20 and the backbone of Phe-234 (3.43Å), halogen interactions between the F atom in ring A with the backbone of Phe-234 (3.56Å) and the two oxygen atoms in Asp-231 (3.09Å and 3.20Å), π-π stacking interactions of ring B with Phe-339 (4.95Å) and the two rings from Trp-336 (4.77Å and 5.45Å), a π-π stacking interaction of the methylenedioxy moiety with Phe-339 (4.13Å), carbon H-bonds between a carbon atom of the methylenedioxy moiety with Ser-239 (3.51Å) and Asn-343 (3.19Å), a carbon H-bond between C12 and Ser-159 (3.49Å) and a conventional H-bond between H21 and Ser-242 (2.20Å).

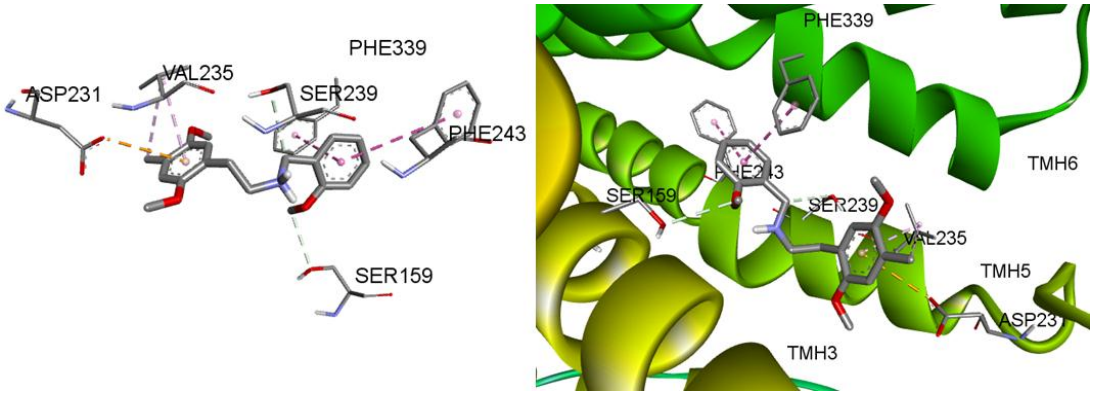

Figure 23: Molecule 13 docked to the 5-HT$_{2A}$ binding site.

We can observe a π-alkyl interaction of ring A with Val-235 (4.17Å), a π-anion interaction of ring A with Asp-231 (4.06Å), an alkyl interaction of the carbon atom of the 5-Me substituent in ring A with Val-235 (4.94Å), a π-π T-shaped interaction of ring B with Phe-339 (4.80Å), a π-π stacking interaction of ring B with Phe-243 (5.71Å), a carbon H-bond between the carbon atom of 2-OMe in ring B and Ser-159 (3.27Å) and a carbon H-bond between C12 and Ser-239 (3.49Å).

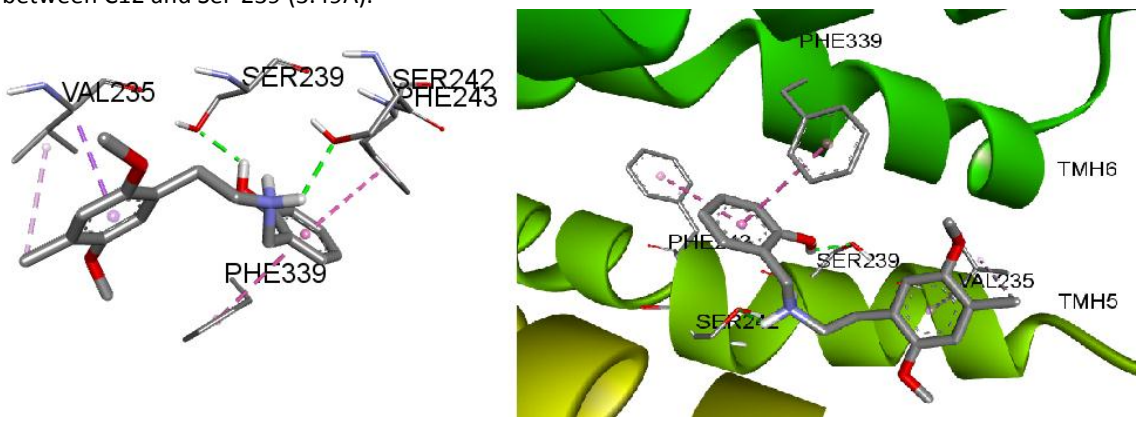

Figure 24: Molecule 14 docked to the 5-HT$_{2A}$ binding site.

We can observe a π-σ interaction of ring A with Val-235 (3.92Å), an alkyl interaction of C from 5-Me in ring A with Val-235 (4.51Å), a π-π T-shaped interaction of ring B with Phe-339 (4.78Å), a π-π stacking interaction of ring B with Phe-243 (5.82Å), a conventional H-bond between H from the 2-OH substituent in ring B with Ser-239 (2.19Å) and a conventional H-bond between H21 and Ser-242 (2.49Å).

ISSN: 0975-8585

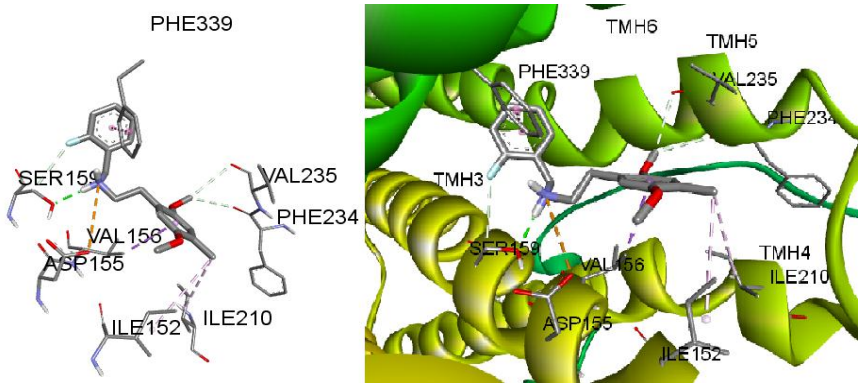

Figure 25: Molecule 15 docked to the 5-HT$_{2A}$ binding site.

We can observe a π-σ interaction of ring A with Val-156 (3.90Å), alkyl interactions of the carbon atom of 5-Me in ring A with Ile-152 (5.29Å) and Ile-210 (4.83Å), carbon H-bonds between C19 with Val-235 (3.48Å) and the backbone of Phe-234 (3.60Å), a π-π T-shaped interaction of ring B with Phe-339 (4.87Å), a carbon H-bond between F in ring B and Ser-159 (3.57Å), a conventional H-bond between H21 and Ser-159 (2.04Å) and an attractive charge interaction between N11 and Asp-155 (5.13Å).

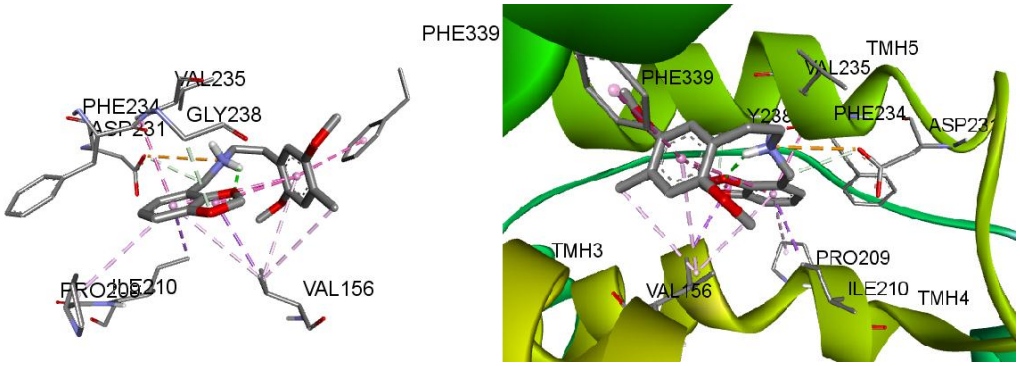

Figure 26: Molecule 16 docked to the 5-HT$_{2A}$ binding site.

Here we can observe a π-alkyl interaction of ring A with Val-156 (4.94Å), π-π T-shaped interaction of ring A with Phe-339 (4.65Å), an alkyl interaction of the carbon atom of the 5-Me substituent in ring A with Val-156 (4.57Å), π-alkyl interactions of ring B with Val-156 (5.11Å) and Pro-209 (5.48Å), a π-σ interaction of ring B with Ile-210 (3.98Å), amide-π stacking interactions of ring B with the backbone of Phe-234 and Val-235 (3.89Å), a π-σ interaction of the methylenedioxy moiety with Val-156 (3.59Å), a carbon H-bond between the oxygen atom of the methylenedioxy moiety and Gly-238 (3.28Å), an attractive charge interaction between N11 and Asp-231 (4.17Å), a carbon H-bond between C12 and Asp-231 (3.45Å). Also, there is an intramolecular π-π T-shaped interaction of ring A with ring B (5.81Å) and with the methylenedioxy moiety (4.40Å) and an intramolecular H-bond between H21 and the O atom from the methylenedioxy moiety (2.13Å).

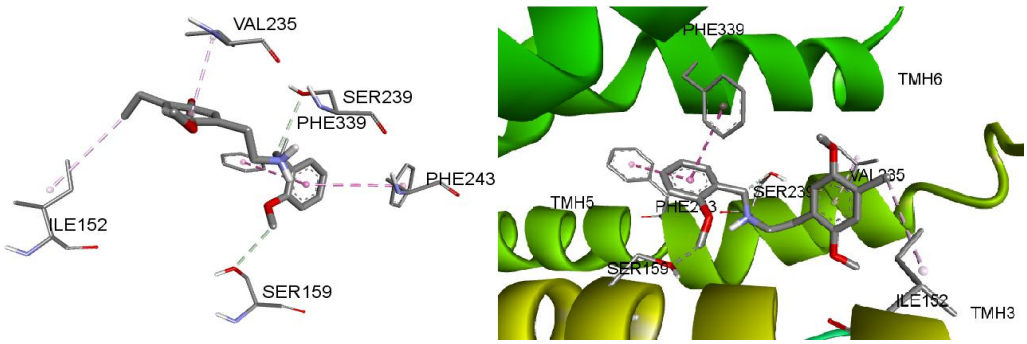

Figure 27: Molecule 17 docked to the 5-HT$_{2A}$ binding site.

Here we can observe a π-alkyl interaction of ring A with Val-235 (4.16Å), an alkyl interaction of the terminal C in the ethyl substituent with Ile-152 (5.19Å), a π-π T-shaped interaction of ring B with Phe-339 (4.81Å), a π-π stacking interaction of ring B with Phe-243 (5.59Å), a carbon H-bond between the Me part from the 2-OMe substituent in ring B and Ser-159 (3.24Å) and a carbon H-bond between C12 and Ser-239 (3.46Å).

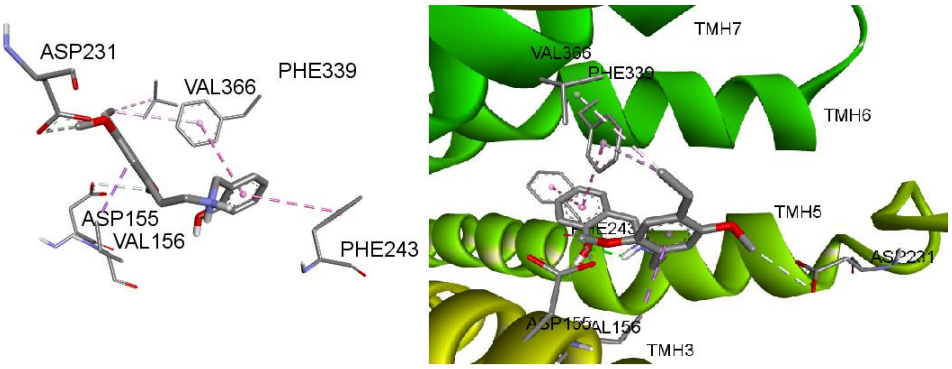

Figure 28: Molecule 18 docked to the 5-HT$_{2A}$ binding site.

We can observe a π-σ interaction of ring A with Val-156 (3.80Å), a carbon H-bond between C19 and Asp-155 (3.31Å), a π-alkyl interaction of the terminal C in the ethyl substituent with Phe-339 (5.09Å), an alkyl interaction of the terminal C in the ethyl substituent with Val-366 (4.46Å), a carbon H-bond between C20 and Asp-231 (3.62Å), a π-π T-shaped interaction of ring B with Phe-339 (4.87Å) and a π-π stacking interaction of ring B with Phe-243 (5.56Å). There is an intramolecular H-bond between H21 and the O atom from the 2-OH substituent in ring B (2.19Å).

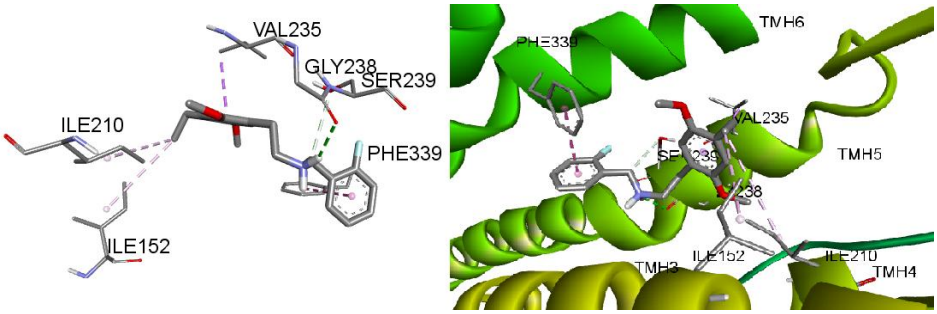

Figure 29: Molecule 19 docked to the 5-HT$_{2A}$ binding site.

Here we may observe a π-σ interaction of ring A with Val-235 (3.96Å), alkyl interactions of the terminal C atom of the ethyl substituent with Ile-210 (5.49Å) and Ile-152 (5.11Å), a π-π T-shaped interaction of ring B and Phe-339 (4.79Å), a conventional H-bond between H21 and Gly-238 (2.67Å) and a carbon H-bond between C12 and Ser-239 (3.65Å).

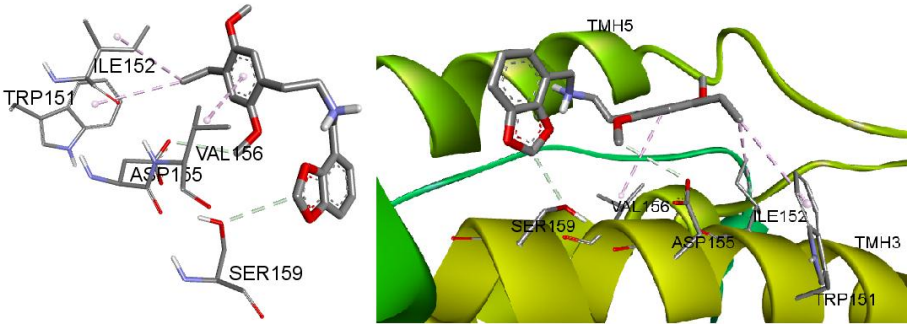

Figure 30: Molecule 20 docked to the 5-HT$_{2A}$ binding site.

In this case we observe a π-alkyl interaction of ring A with Val-156 (4.98Å), a carbon H-bond between C19 and Asp-155 (3.42Å), a π-alkyl interaction of the terminal carbon atom of the ethyl substituent with Trp-

151 (4.81Å), an alkyl interaction of the terminal C atom from the ethyl substituent with Ile-152 (4.80Å) and a carbon H-bond between the C atom of the methylenedioxy moiety and Ser-159 (3.48Å).

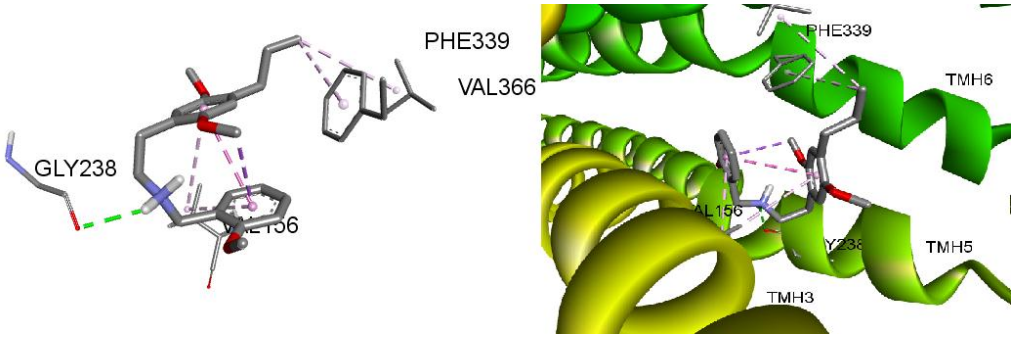

Figure 31: Molecule 21 docked to the 5-HT$_{2A}$ binding site.

Here we observe a π-alkyl interaction of ring A with Val-156 (5.40Å), a π-alkyl interaction of the terminal C atom of the ethyl substituent with Phe-339 (4.99Å), an alkyl interaction of the terminal C atom of the ethyl substituent with Val-366 (4.66Å), a π-alkyl interaction of ring B with Val-156 (4.66Å) and a conventional H-bond between H21 and Gly-238 (2.48Å). There is one intramolecular π-π stacking interaction of ring A with ring B (4.37Å) and another intramolecular π-σ interaction of C19 with ring B (3.99Å).

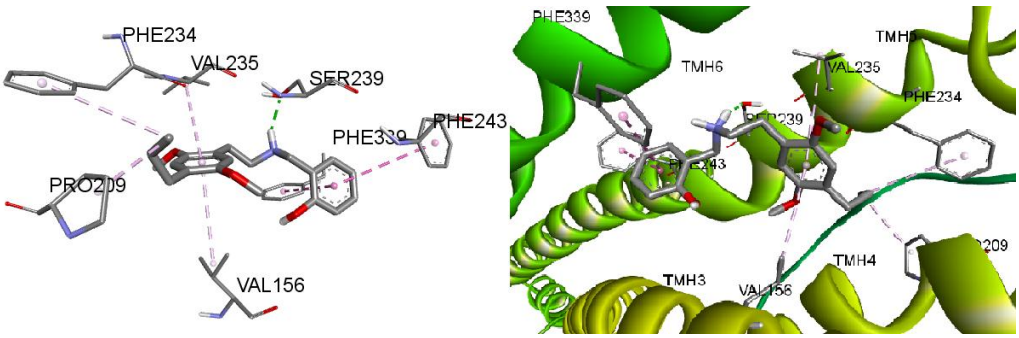

Figure 32: Molecule 22 docked to the 5-HT$_{2A}$ binding site.

Here we can observe π-alkyl interactions of ring A with Val-156 (4.84Å) and Val-235 (5.13Å), a π-alkyl interaction of the terminal C atom from the propyl substituent with Phe-234 (5.46Å), an alkyl interaction of the terminal C from the propyl substituent with Pro-209 (3.98Å), a π-π T-shaped interaction of ring B with Phe-339 (4.90Å), a π-π stacking interaction of ring B with Phe-243 (5.68Å) and a conventional H-bond between H21 and Ser-239 (2.14Å).

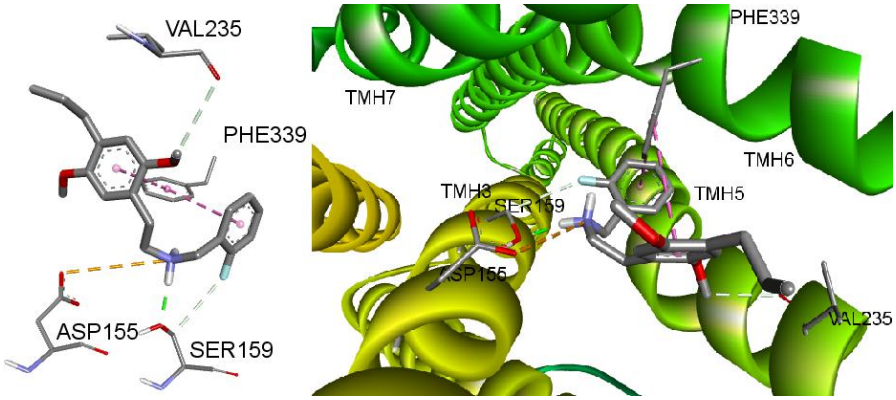

Figure 33: Molecule 23 docked to the 5-HT$_{2A}$ binding site.

We can observe here a π-π T-shaped interaction of ring A with Phe-339 (4.94Å), a carbon H-bond between C19 and Val-235 (3.36Å), a π-π T-shaped interaction of ring B with Phe-339 (4.78Å), a carbon H-bond

between the fluorine atom in ring B and Ser-159 (3.65Å), a conventional H-bond between H21 and Ser-159 (1.97Å) and an attractive charge interaction of N11 with Asp-155 (5.08Å).

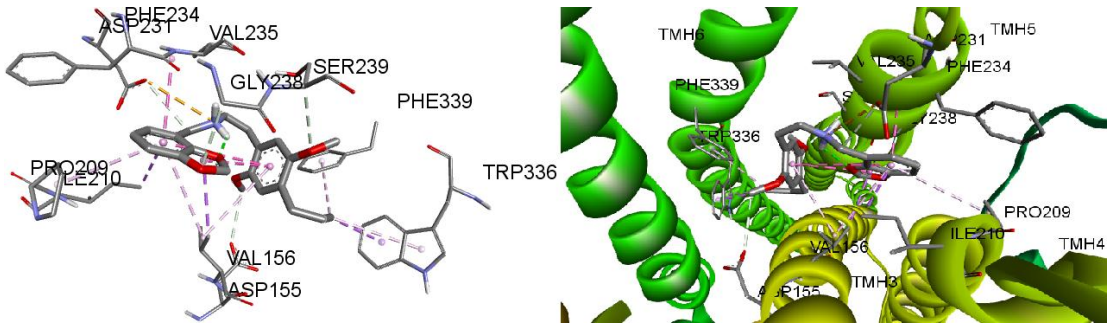

Figure 34: Molecule 24 docked to the 5-HT$_{2A}$ binding site.

Here we can observe a π-alkyl interaction of ring A with Val-156 (4.95Å), π-alkyl interactions of the terminal C atom of the propyl substituent with Phe-339 (4.91Å) and the pyrrole moiety in Trp-336 (5.05Å), a π-σ interaction of the terminal C atom of the propyl substituent with the phenyl moiety in Trp-336 (3.88Å), a carbon H-bond between O8 and Ser-239 (3.64Å), a carbon H-bond between C19 and Asp-155 (3.22Å), π-alkyl interactions of ring B with Val-156 (5.15Å) and Pro-209 (5.44Å), a π-σ interaction of ring B with Ile-210 (3.99Å), amide-π stacking interactions of ring B with the backbone of Phe-234 and Val-235 (3.88Å), a π-σ interaction of the methylenedioxy moiety and Val-156 (3.61Å), a carbon H-bond between the O atom from the methylenedioxy moiety and Gly-238 (3.26Å), an attractive charge interaction of N11 and Asp-231 (4.24Å) and a carbon H-bond between C12 and Asp-231 (3.48Å). Also, there is an intramolecular π-π T-shaped interaction of ring A with ring B (5.81Å) and the methylenedioxy moiety (4.36Å) and an intramolecular H-bond between H21 and the O atom from the methylenedioxy moiety (2.11Å).

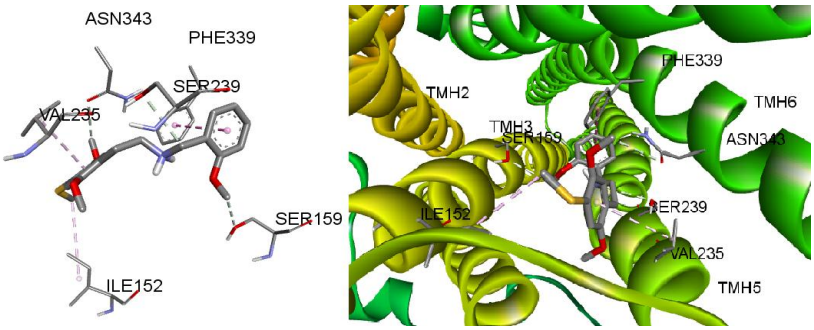

Figure 35: Molecule 25 docked to the 5-HT$_{2A}$ binding site.

Here we can observe a π-alkyl interaction of ring A with Val-235 (4.45Å), an alkyl interaction of the C atom from 5-SMe with Ile-152 (5.14Å), a carbon H-bond between C19 and Asn-343 (3.53Å), a π-π T-shaped interaction of ring B with Phe-339 (4.81Å), a carbon H-bond between the C atom from the 2-OMe substituent in ring B and Ser-159 (3.37Å) and carbon H-bond between C12 and Ser-239 (3.47Å).

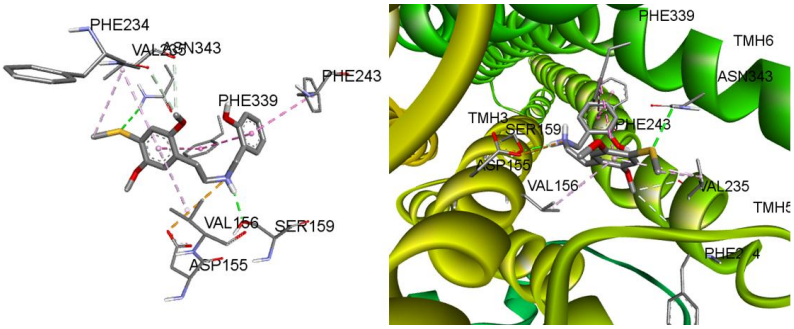

Figure 36: Molecule 26 docked to the 5-HT$_{2A}$ binding site.

We can observe π-alkyl interactions of ring A with Val-156 (5.44Å) and Val-235 (5.48Å), a π-π T-shaped interaction of ring A with Phe-339 (5.18Å), carbon H-bonds between C19 and the backbone of Phe-234 (3.60Å) and Val-235 (3.52Å), a conventional H-bond between the S atom of 5-SMe and Asn-343 (3.00Å), an alkyl interaction of the C atom from 5-SMe and Val-235 (4.93Å), a π-π-T shaped interaction of ring B with Phe-339 (4.78Å), a π-π stacking interaction of ring B with Phe-243 (5.49Å), a conventional H-bond between H21 and Ser-159 (2.03Å) and an attractive charge interaction of N11 with Asp-155 (5.31Å).

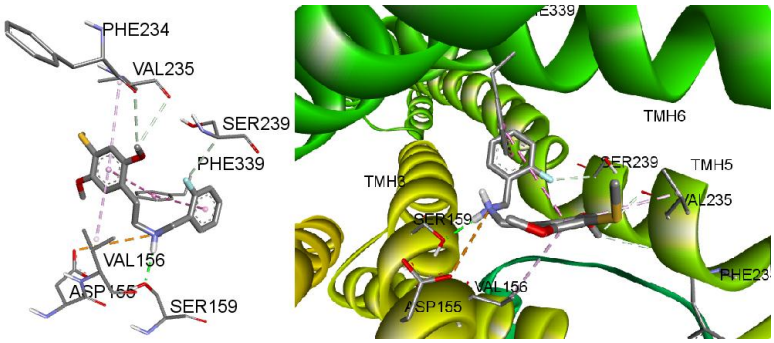

Figure 37: Molecule 27 docked to the 5-HT$_{2A}$ binding site.

We can observe π-alkyl interactions of ring A with Val-156 (5.32Å) and Val-235 (5.41Å), a π-π T-shaped interaction of ring A with Phe-339 (5.41Å), carbon H-bonds between C19 and the backbone of Phe-234 (3.39Å) and Val-235 (3.53Å), a π-π T-shaped interaction of ring B with Phe-339 (4.84Å), a carbon H-bond between the F atom in ring B and Ser-239 (3.50Å), a conventional H-bond between H21 and Ser-159 (2.03Å) and an attractive charge interaction of N11 with Asp-155 (5.34Å).

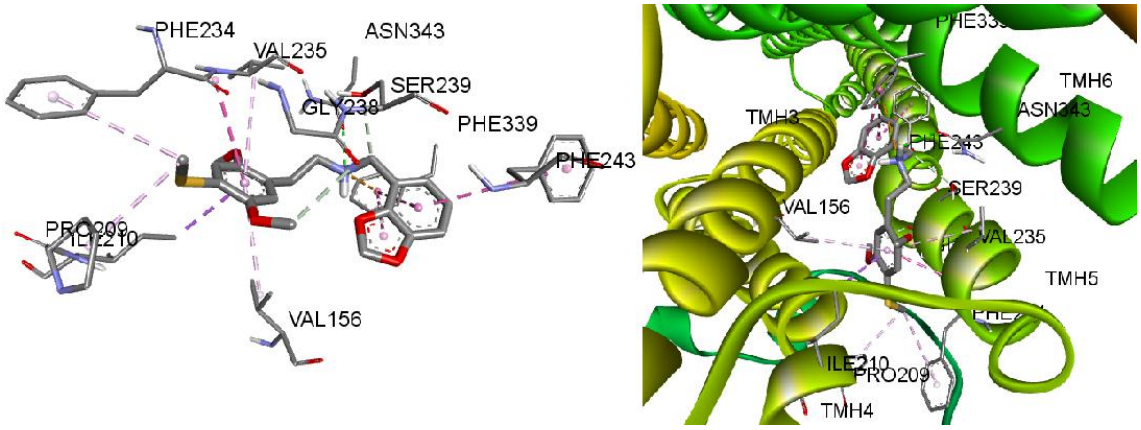

Figure 38: Molecule 28 docked to the 5-HT$_{2A}$ binding site.

Here we can observe π-alkyl interactions of ring A with Val-156 (4.57Å) and Val-235 (5.46Å), amide-π stacking interactions of ring A with the backbone of Phe-234 and Val-235 (4.29Å), a π-σ interaction of ring A with Ile-210 (3.96Å), an alkyl interaction of the C atom of 5-SMe with Pro-209 (4.01Å), a π-alkyl interaction of the C atom of 5-SMe with Phe-234 (5.08Å), a carbon H-bond between C20 and Gly-238 (3.30Å), π-π stacking interactions of ring B with Phe-243 (5.98Å) and Phe-339 (4.97Å), a π-π stacking interaction of the methylenedioxy moiety with Phe-339 (5.92Å), a carbon H-bond between C12 and Ser-239 (3.31Å), a conventional H-bond between H21 and Asn-343 (2.40Å) and a π-cation interaction of N11 with Phe-339 (4.03Å).

ISSN: 0975-8585

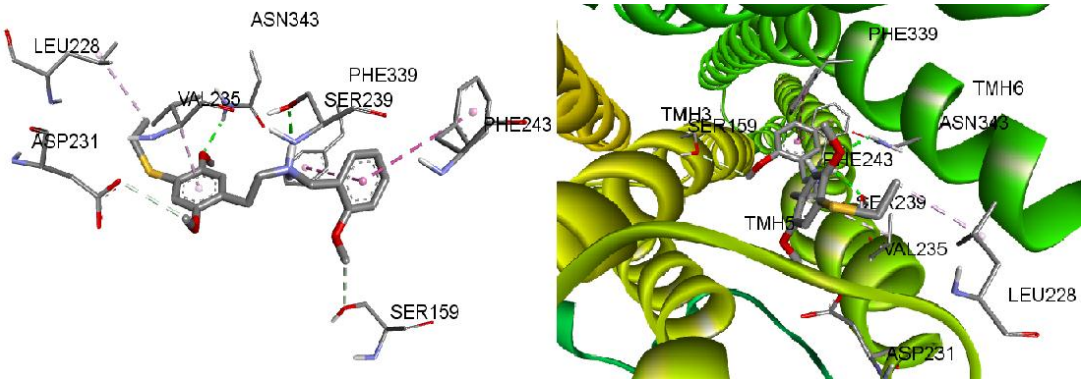

Figure 39: Molecule 29 docked to the 5-HT$_{2A}$ binding site.

We can observe a π-alkyl interaction of ring A with Val-235 (4.30Å), a conventional H-bond between O8 and Asn-343 (2.03Å), an alkyl interaction of the terminal C atom from 5-SEt with Leu-228 (4.01Å), a carbon H-bond between C19 and Asp-231 (3.27Å), a π-π T-shaped interaction of ring B with Phe-339 (4.84Å), a π-π stacking interaction of ring B with Phe-243 (5.65Å), a carbon H-bond between the C atom of the 2-OMe substituent in ring B with Ser-159 (3.35Å) and a conventional H-bond between H21 and Ser-239 (2.45Å).

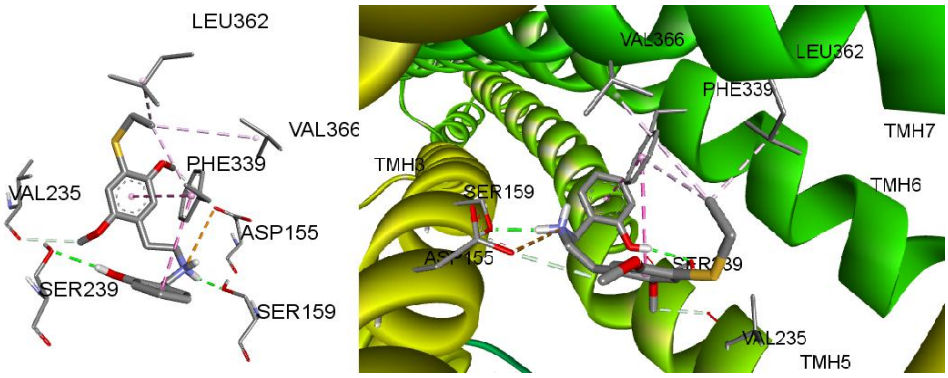

Figure 40: Molecule 30 docked to the 5-HT$_{2A}$ binding site.

We observe here a π-π T-shaped interaction of ring A with Phe-339 (5.00Å), a π-alkyl interaction of the terminal C atom from 5-SEt with Phe-339 (4.69Å), alkyl interactions of the terminal C from 5-SEt with Val-366 (5.14Å) and Leu-362 (4.07Å), a carbon H-bond between C20 and Asp-155 (3.46Å), a carbon H-bond between C19 and Val-235 (3.31Å), a π-π T-shaped interaction of ring B with Phe-339 (4.80Å), a conventional H-bond between the H atom from the 2-OH substituent in ring B and Ser-239 (2.36Å), a conventional H-bond between H21 and Ser-159 (2.01Å) and an attractive charge interaction of N11 with Asp-155 (5.32Å).

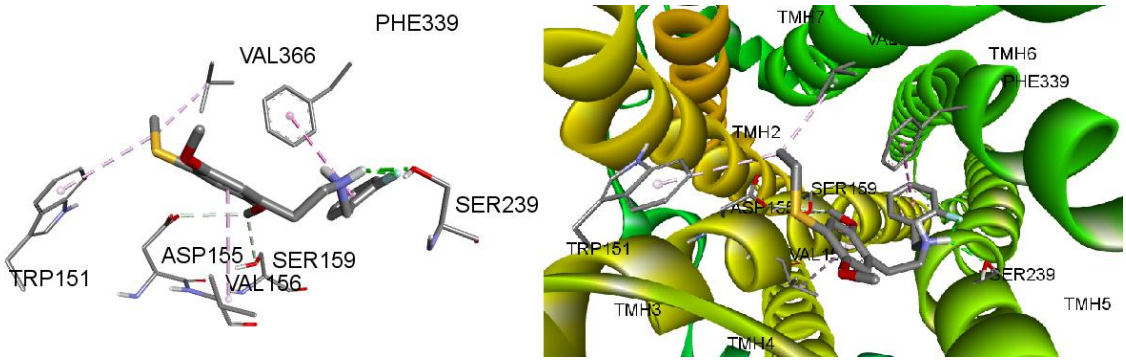

Figure 41: Molecule 31 docked to the 5-HT$_{2A}$ binding site.

We can observe a π-alkyl interaction of ring A with Val-156 (4.93Å), a π-alkyl interaction of the terminal C of 5-SEt with Trp-151 (4.91Å), a alkyl interaction of the terminal C atom of 5-SEt with Val-366

(4.17Å), carbon H-bonds between C19 and Asp-155 (3.45Å) and Ser-159 (3.53Å), a π-π T-shaped interaction of ring B with Phe-339 (4.78Å) and a conventional H-bond between H21 and Ser-239 (2.12Å). There is an intramolecular H-bond between H21 and F in ring B (2.44Å).

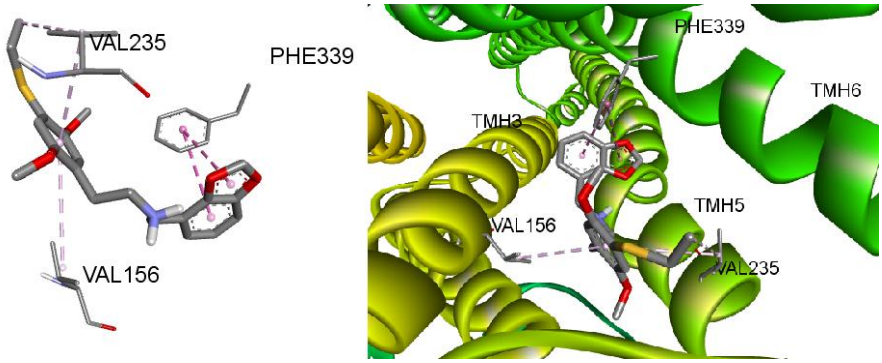

Figure 42: Molecule 32 docked to the 5-HT$_{2A}$ binding site.

Here we can observe π-alkyl interactions of ring A with Val-156 (5.22Å) and Val-235 (5.03Å) and π-π T-shaped interactions of ring B and the methylenedioxy moiety with Phe-339 (4.83Å and 4.93Å, respectively).

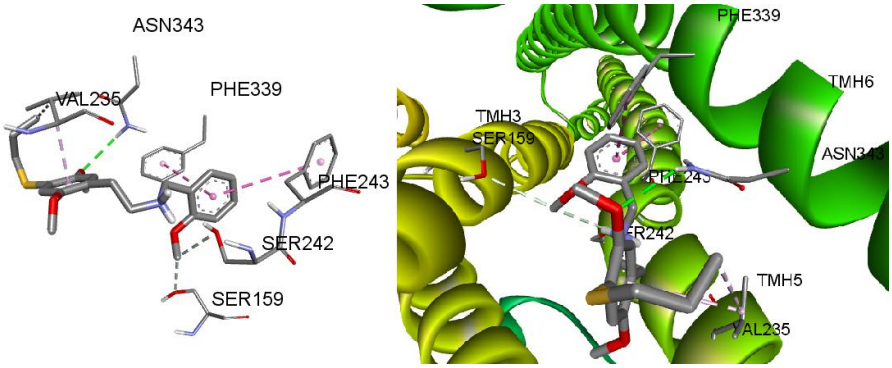

Figure 43: Molecule 33 docked to the 5-HT$_{2A}$ binding site.

Here we can observe a π-alkyl interaction of ring A with Val-235 (4.38Å), an alkyl interaction of the terminal C atom of 5-SPr with Val-235 (4.26Å), a conventional H-bond between O8 and Asn-343 (2.78Å), a π-π T-shaped interaction of ring B with Phe-339 (4.83Å), a π-π stacking interaction of ring B with Phe-243 (5.76Å) and carbon H-bonds between the C atom of 2-OMe in ring B with Ser-159 (3.30Å) and Ser-242 (3.79Å).

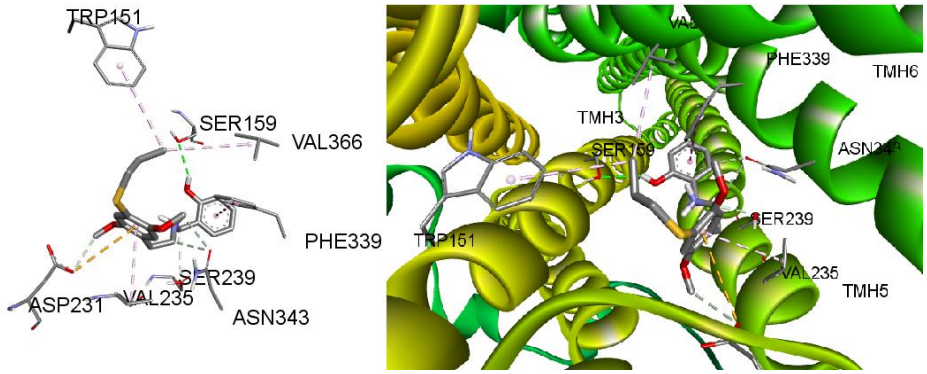

Figure 44: Molecule 34 docked to the 5-HT$_{2A}$ binding site.

We can observe a π-alkyl interaction of ring A with Val-235 (4.41Å), a π-anion interaction of ring A with Asp-231 (4.72Å), a carbon H-bond between C19 and Asp-231 (3.33Å), a carbon H-bond between C20 and Asn-343 (3.74Å), a π-alkyl interaction of the terminal C atom of 5-SPr with Trp-151 (5.30Å), an alkyl interaction

of the terminal C atom of 5-SPr with Val-366 (4.92Å), a π-π T shaped interaction of ring B with Phe-339 (4.85Å), a conventional H-bond between the H atom of the 2-OH substituent in ring B and Ser-159 (2.78Å), a carbon H-bond between C12 and Ser-239 (3.66Å) and a carbon H-bond between C10 and Asn-343 (3.49Å).

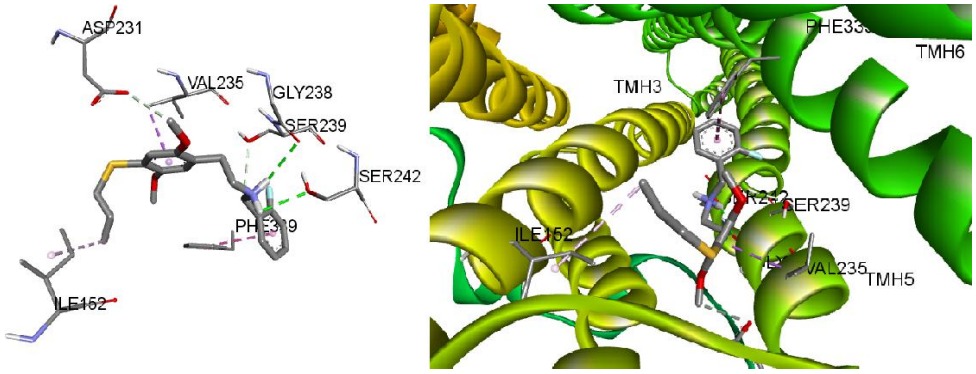

Figure 45: Molecule 35 docked to the 5-HT$_{2A}$ binding site.

Here we can observe a π-σ interaction of ring A with Val-235 (3.98Å), an alkyl interaction of the terminal C atom of 5-SPr with Ile-152 (4.98Å), a carbon H-bond between C19 and Asp-231 (3.77Å), a π-π T-shaped interaction of ring B with Phe-339 (4.88Å), a carbon H-bond between C12 and Ser-239 (3.68Å), a conventional H-bond between H21 and Gly-238 (2.68Å) and a conventional H-bond between one hydrogen from the amine group and Ser-242 (2.76Å).

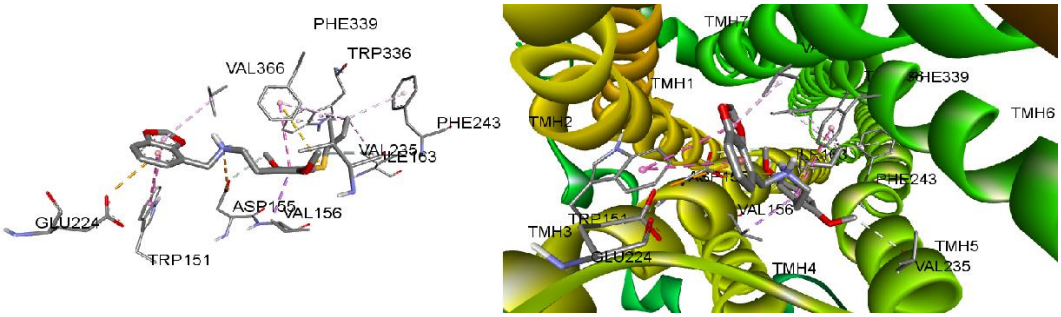

Figure 46: Molecule 36 docked to the 5-HT$_{2A}$ binding site.

We can observe a π-π T-shaped interaction of ring A with Phe-339 (4.84Å), a π-σ interaction of ring A with Val-156 (3.63Å), a carbon H-bond between C19 and Val-235 (3.71Å), a π-sulfur interaction of the S atom of 5-SPr with Phe-339 (5.59Å), π-alkyl interactions of the terminal C atom of 5-SPr with Phe-339 (5.09Å), Trp-336 (4.49Å and 4.63Å) and Phe-243 (4.50Å), an alkyl interaction of the terminal C atom of 5-SPr with Ile-163 (5.40Å), a carbon H-bond between C20 and Asp-155 (3.42Å), π-π T-shaped interactions of ring B with the methylenedioxy moiety and with Phe-339 (5.22Å and 5.00Å, respectively), a π-anion interaction of ring B with Glu-224 (3.89Å), a π-alkyl interaction of the methylenedioxy moiety with Val-366 (4.71Å) and an attractive charge interaction of N11 with Asp-155 (4.57Å).

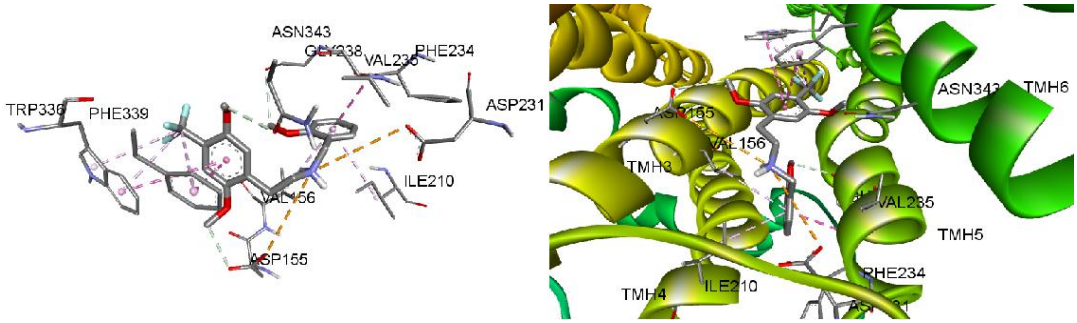

Figure 47: Molecule 37 docked to the 5-HT$_{2A}$ binding site.

We can observe π-π stacking interactions of ring A with Phe-339 (4.18Å) and Trp-336 (5.68Å), a carbon H-bond between C19 and Asp-155 (3.06Å), π-alkyl interactions of the C atom of 5-CF_3 with Phe-339 (5.09Å) and Trp-336 (5.14Å and 4.48Å), a carbon H-bond between C20 and Asn-343, π-alkyl interactions of ring B with Ile-210 (5.12Å) and Val-156 (4.75Å), amide-π interactions of ring B with the backbone of Phe-234 and Val-235 (4.03Å), a carbon H-bond between the C atom of the 2-OMe substituent in ring B and Gly-238 (3.55Å) and attractive charge interactions of N11 with Asp-155 (5.39Å) and Asp-231 (5.52Å).

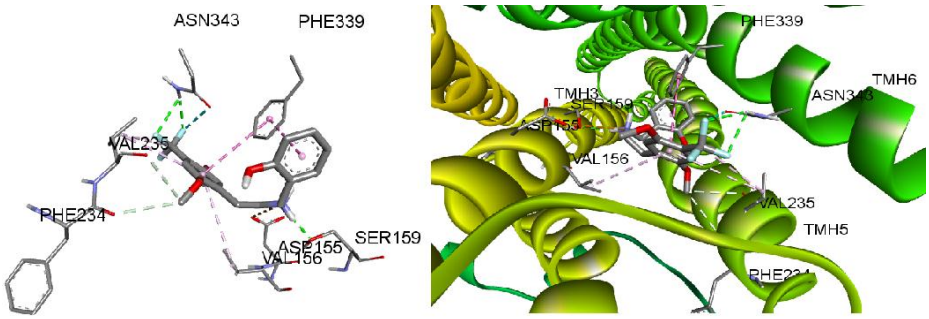

Figure 48: Molecule 38 docked to the 5-HT_{2A} binding site.

We can observe a π-π T-shaped interaction of ring A with Phe-339 (5.10Å), π-alkyl interactions of ring A with Val-235 (5.44Å) and Val-156 (5.50Å), carbon H-bonds between C19 with the backbone of Phe-234 (3.58Å) and the backbone of Val-235 (3.50Å), conventional H-bonds (halogen) between two F atoms of the 5-CF_3 substituent and Asn-343 (2.69Å and 2.43Å), a halogen interaction of one fluorine atom of 5-CF_3 with Asn-343 (3.58Å), a π-π T-shaped interaction of ring B with Phe-339 (4.79Å), a conventional H-bond between H21 and Ser-159 (2.02Å) and an attractive charge interaction of N11 and Asp-155 (5.34Å).

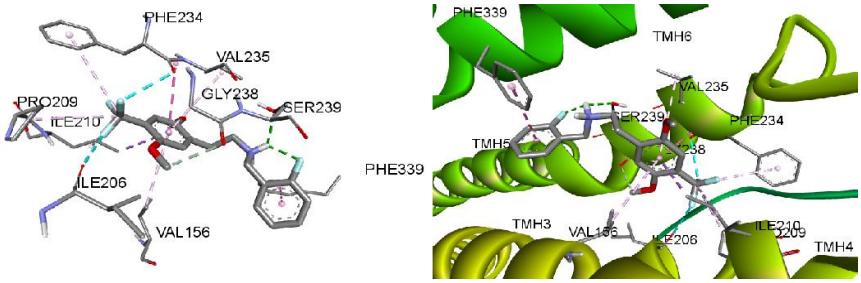

Figure 49: Molecule 39 docked to the 5-HT_{2A} binding site.

We can observe π-alkyl interactions of ring A with Val-156 (4.73Å) and Val-235 (5.40Å), a π-σ interactions of ring A with Ile-210 (3.99Å), amide-π interactions of ring A with the backbones of Phe-234 and Val-235 (4.09Å), alkyl interactions of the C atom from 5-CF_3 with Ile-210 (4.61Å) and Pro-209 (4.40Å), a π-alkyl interactions of C from 5-CF_3 and Phe-234 (5.30Å), a halogen interaction of one F atom from 5-CF_3 with Ile-206 (3.01Å), a halogen interaction of one F from 5-CF_3 with Phe-234 (3.17Å), a carbon H-bond between C20 and Gly-238 (3.40Å), a π-π T-shaped interaction of ring B with Phe-339 (4.81Å) and a conventional H-bond between H21 and Ser-239 (2.68Å). There is also an intramolecular H-bond between H21 and the F substituent in ring B (2.57Å).

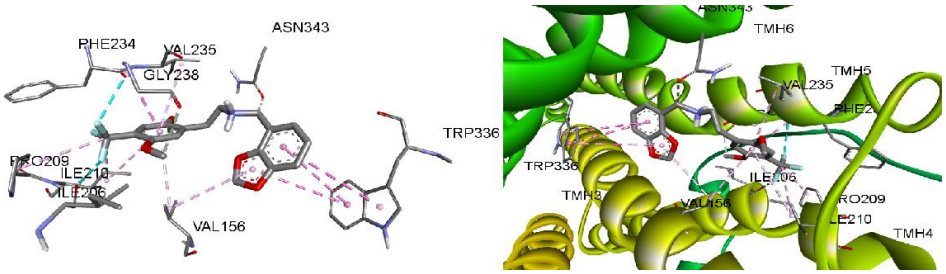

Figure 50: Molecule 40 docked to the 5-HT_{2A} binding site.

Here we can observe π-alkyl interactions of ring A with Val-156 (4.79Å), Val-235 (5.25Å) and Ile-210 (5.49Å), amide-π interactions of ring A with the backbone of Phe-234 and Val-235 (4.11Å), alkyl interactions of the C atom of 5-CF_3 with Ile-210 (4.64Å) and Pro-209 (4.56Å), a halogen interaction of one F atom of 5-CF_3 with Ile-206 (2.98Å), a halogen interaction of one F atom of 5-CF_3 with Phe-234 (3.15Å), a carbon H-bond between C20 and Gly-238 (3.32Å), a π-π stacking interaction of ring B with Trp-336 (5.85Å and 5.02Å), a π-π stacking interaction of the methylenedioxy moiety with Trp-336 (5.63Å) and a π-alkyl interaction of the methylenedioxy moiety with Val-156 (5.25Å).

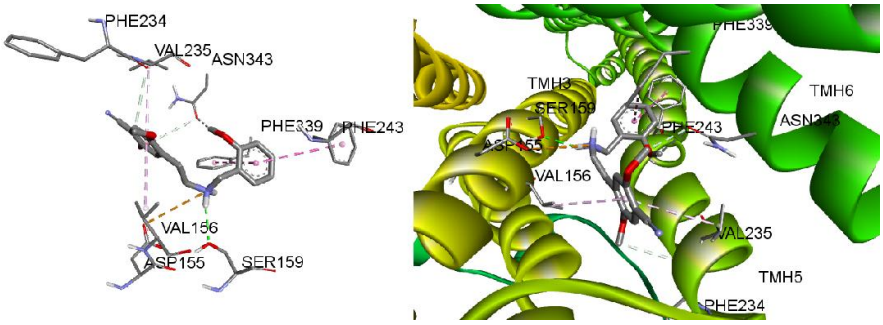

Figure 51: Molecule 41 docked to the 5-HT_{2A} binding site.

We can observe π-alkyl interactions of ring A with Val-156 (5.05Å) and Val-235 (5.17Å), a carbon H-bond between C19 and the backbone of Phe-234 (3.77Å), a carbon H-bond between C20 and Asn-343 (3.58Å), a π-π T-shaped interaction of ring B with Phe-339 (4.83Å), a π-π stacking interaction of ring B with Phe-243 (5.58Å), a carbon H-bond between the C atom of 2-OMe in ring B and Asn-343 (3.43Å), a conventional H-bond between H21 and Ser-159 (2.36Å) and an attractive charge interaction of N11 with Asp-155 (5.27Å).

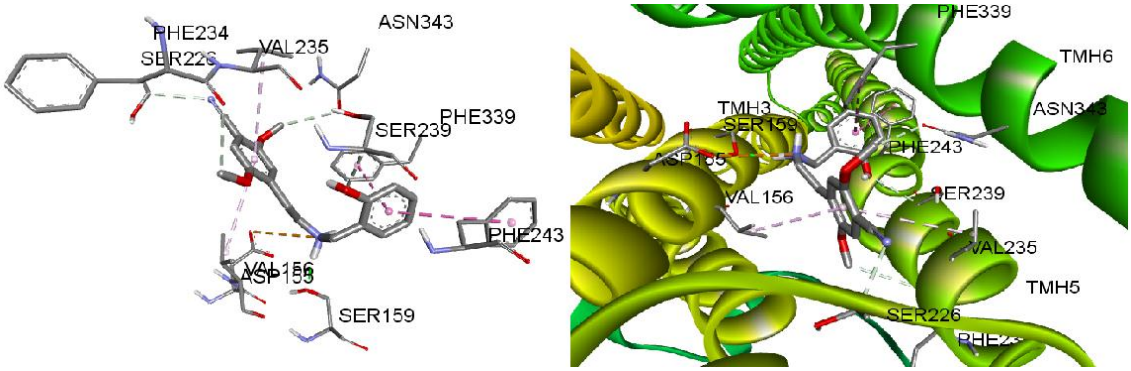

Figure 52: Molecule 42 docked to the 5-HT_{2A} binding site.

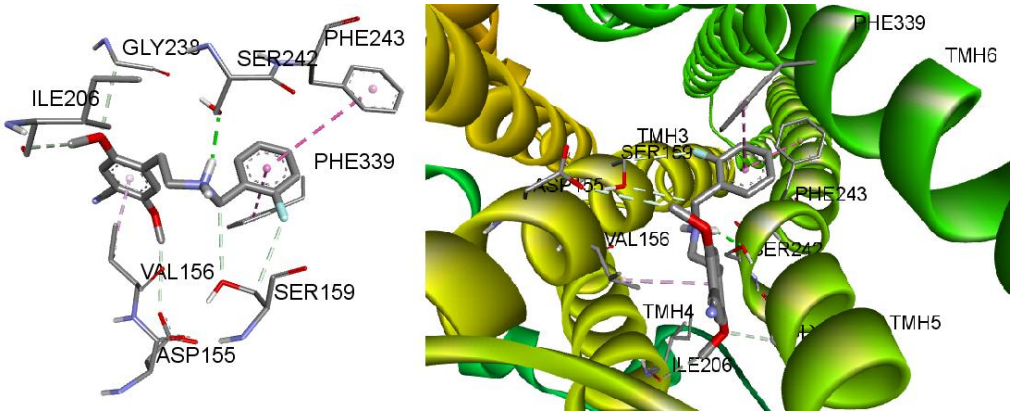

Figure 53: Molecule 43 docked to the 5-HT_{2A} binding site.

ISSN: 0975-8585

In this case we observe π-alkyl interactions of ring A with Val-156 (4.84Å) and Val-235 (5.42Å), a carbon H-bond between C19 and Phe-234 (3.62Å), a carbon H-bond between the N atom of the 5-CN substituent and Ser-226 (3.24Å), a carbon H-bond between C20 and Asn-343 (3.52Å), a π-π T-shaped interaction of ring B with Phe-339 (4.93Å), a π-π stacking interaction of ring B with Phe-243 (5.52Å), a carbon H-bond between the O atom of 2-OH in ring B and Ser-239 (3.48Å), a conventional H-bond between H21 and Ser-159 (1.98Å) and an attractive charge interaction of N11 and Asp-155 (5.28Å).

We can observe a π-alkyl interaction of ring A with Val-156 (4.45Å), a carbon H-bond between O7 and Gly-238 (3.28Å), a carbon H-bond between C19 and Ile-206 (3.50Å), a carbon H-bond between C20 and Asp-155 (3.78Å), a π-π T-shaped interaction of ring B with Phe-339 (4.80Å), a π-π stacking interaction of ring B with Phe-243 (5.82Å), a carbon H-bond between the F substituent in ring B and Ser-159 (3.61Å), a carbon H-bond between C12 and Ser-159 (3.61Å) and a conventional H-bond between H21 and Ser-242 (2.13Å).

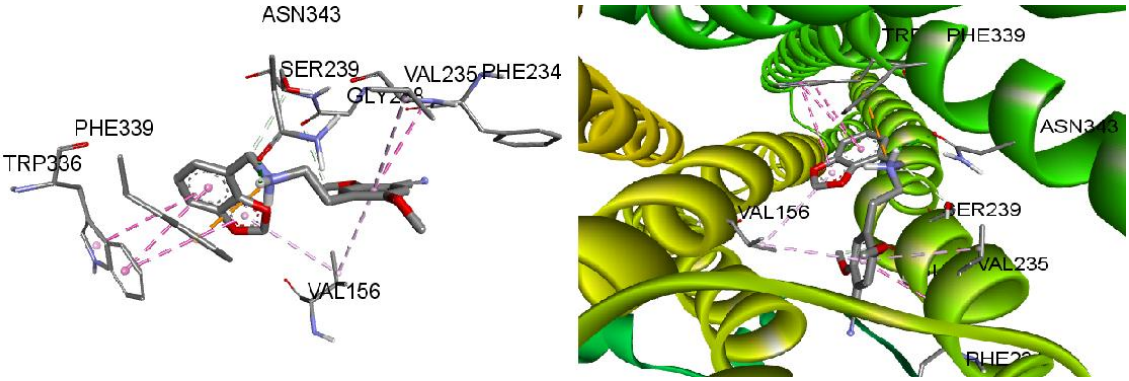

Figure 54: Molecule 44 docked to the 5-HT_{2A} binding site.

We can observe π-alkyl interactions of ring A with Val-156 (4.75Å) and Val-235 (5.18Å), amide-π interactions of ring A with the backbone of Phe-234 and Val-235 (4.25Å), a carbon H-bond between C20 and the backbone of Gly-238 (3.32Å), π-π stacking interactions of ring B with two rings from Trp-336 (4.97Å and 5.75Å), a π-π stacking interaction of the methylenedioxy moiety with Trp-336 (5.64Å), a π-alkyl interaction of the methylenedioxy with Val-156 (5.37Å), a carbon H-bond between C12 and Ser-239 (3.21Å), a conventional H-bond between H21 and Asn-343 (2.14Å) and a π-cation interaction of N11 with Phe-339 (3.88Å).

A general conclusion is that these molecules have several different modes of binding to the 5-HT_{2A} receptor. Considering the number and kinds of interactions together with the relative orientation of the molecules inside the binding site, we may build two or three sets comprising two or more molecules. What is of paramount importance here is the degree of validity of the methods employed in this work. Today there is a little doubt that the LMRA results provide good quality information about the ligand-receptor binding. The problem is that the information depends on factors such as the number of molecules under study and the kind of common skeleton employed. On the other hand, docking results are fully compatible with LRMA results and provide more data about the nature of the possible ligand-site interactions. A strategy allowing connecting both methods is needed. We did not compare our results with other docking studies due to differences in the model and software. There is a central question about the relationship between, for example, the dose for reaching a "basic hallucinatory" experience and not an internal "trip" like the one obtained with LSD (the "trip" obviously depends on the *contents* of the "mind"). Considering that we are primates it would be possible in theory to build a "primate hallucination scale" based uniquely on the kinds of distortions of the "external world" and relate it to the dose needed to achieve only those effects. This analysis has not been done and we feel that we have not yet the tools to do it [78]. A set of high resolution images in png format of all docking figures is available on request via DropBox only.

REFERENCES

[1] A Shulgin; A Shulgin, Pihkal: A Chemical Love Story, Transform Press, USA, 1991.
[2] A Shulgin; A Shulgin, Tihkal: The Continuation, Transform Press, USA, 1997.
[3] G Appendino; A Minassi; O Taglialatela-Scafati, Nat. Prod. Rev., 2014, 31, 880-904.

[4] A Bosak; F LoVecchio; M Levine, J. Med. Toxicol., 2013, 9, 196-198.
[5] SL Hill; T Doris; S Gurung; S Katebe; A Lomas, et al., Clin. Toxicol., 2013, 51, 487-492.
[6] P Nikolaou; I Papoutsis; M Stefanidou; C Spiliopoulou; S Athanaselis, Drug Chem. Toxicol., 2015, 38, 113-119.
[7] SR Rose; JL Poklis; A Poklis, Clin. Toxicol., 2013, 51, 174-177.
[8] YNA Soh; S Elliott, Drug. Test. Anal., 2014, 6, 696-704.
[9] S Stellpflug; S Kealey; C Hegarty; G Janis, J. Med. Toxicol., 2014, 10, 45-50.
[10] J Suzuki; JL Poklis; A Poklis, J. Psychoact. Drugs, 2014, 46, 379-382.
[11] Y Umemura; T Andrew; V Jacobs; A Giustini; L Lewis, et al., Neurol., 2014, 82, P1.342.
[12] JS Gómez-Jeria, Acta sud Amer. Quím., 1984, 4, 1-9.
[13] JS Gómez-Jeria; D Morales-Lagos, "The mode of binding of phenylalkylamines to the Serotonergic Receptor," in QSAR in design of Bioactive Drugs, M. Kuchar Ed., pp. 145-173, Prous, J.R., Barcelona, Spain, 1984.
[14] JS Gómez-Jeria; DR Morales-Lagos, J. Pharm. Sci., 1984, 73, 1725-1728.
[15] BK Cassels; JS Gómez-Jeria, J. Psychoact. Drugs, 1985, 17, 129-130.
[16] JS Gómez-Jeria; D Morales-Lagos; JI Rodriguez-Gatica; JC Saavedra-Aguilar, Int. J. Quant. Chem., 1985, 28, 421-428.
[17] JS Gómez-Jeria; BK Cassels; RE Clavijo; V Vargas; R Quintana; JC Saavedra-Aguilar, Microgram (DEA), 1986, 19, 153-162.
[18] JS Gómez-Jeria; D Morales-Lagos; BK Cassels; JC Saavedra-Aguilar, Quant. Struct.-Relat., 1986, 5, 153-157.
[19] JS Gómez-Jeria; BK Cassels; JC Saavedra-Aguilar, Eur. J. Med. Chem., 1987, 22, 433-437.
[20] P Richter; A Morales; JS Gomez-Jeria; D Morales-Lagos, Analyst, 1988, 113, 859-863.
[21] JS Gómez-Jeria; A Robles-Navarro, Submitted, 2015,
[22] M Hansen, "Design and Synthesis of Selective Serotonin Receptor Agonists for Positron Emission Tomography Imaging of the Brain," Faculty of Pharmaceutical Sciences, PhD Thesis, pp. 227, University of Copenhagen, Copenhagen, 2010.
[23] JS Gómez-Jeria; A Robles-Navarro, Der Pharma Chem., 2015, In press.,
[24] JS Gómez-Jeria, Int. J. Quant. Chem., 1983, 23, 1969-1972.
[25] JS Gómez-Jeria, "Modeling the Drug-Receptor Interaction in Quantum Pharmacology," in Molecules in Physics, Chemistry, and Biology, J. Maruani Ed., vol. 4, pp. 215-231, Springer Netherlands, 1989.
[26] JS Gómez-Jeria; M Ojeda-Vergara, J. Chil. Chem. Soc., 2003, 48, 119-124.
[27] JS Gómez-Jeria, J. Chil. Chem. Soc., 2009, 54, 482-485.
[28] JS Gómez-Jeria, Elements of Molecular Electronic Pharmacology (in Spanish), Ediciones Sokar, Santiago de Chile, 2013.
[29] JS Gómez-Jeria, Canad. Chem. Trans., 2013, 1, 25-55.
[30] K Fukui; H Fujimoto, Frontier orbitals and reaction paths: selected papers of Kenichi Fukui, World Scientific, Singapore; River Edge, N.J., 1997.
[31] JS Gómez-Jeria; L Espinoza, Bol. Soc. Chil. Quím., 1982, 27, 142-144.
[32] JS Gómez-Jeria; P Sotomayor, J. Mol. Struct. (Theochem), 1988, 166, 493-498.
[33] JS Gómez-Jeria; M Ojeda-Vergara; C Donoso-Espinoza, Mol. Engn., 1995, 5, 391-401.
[34] JS Gómez-Jeria; L Lagos-Arancibia, Int. J. Quant. Chem., 1999, 71, 505-511.
[35] JS Gómez-Jeria; L Lagos-Arancibia; E Sobarzo-Sánchez, Bol. Soc. Chil. Quím., 2003, 48, 61-66.
[36] JS Gómez-Jeria; F Soto-Morales; G Larenas-Gutierrez, Ir. Int. J. Sci., 2003, 4, 151-164.
[37] JS Gómez-Jeria; LA Gerli-Candia; SM Hurtado, J. Chil. Chem. Soc., 2004, 49, 307-312.
[38] F Soto-Morales; JS Gómez-Jeria, J. Chil. Chem. Soc., 2007, 52, 1214-1219.
[39] JS Gómez-Jeria; F Soto-Morales; J Rivas; A Sotomayor, J. Chil. Chem. Soc., 2008, 53, 1393-1399.
[40] JS Gómez-Jeria, J. Chil. Chem. Soc., 2010, 55, 381-384.
[41] T Bruna-Larenas; JS Gómez-Jeria, Int. J. Med. Chem., 2012, 2012 Article ID 682495, 1-16.
[42] JS Gómez-Jeria, Der Pharm. Lett., 2014, 6., 95-104.
[43] JS Gómez-Jeria, SOP Trans. Phys. Chem., 2014, 1, 10-28.
[44] JS Gómez-Jeria, Res. J. Pharmac. Biol. Chem. Sci., 2014, 5, 2124-2142.
[45] JS Gómez-Jeria, J. Comput. Methods Drug Des., 2014, 4, 32-44.
[46] JS Gómez-Jeria, Res. J. Pharmac. Biol. Chem. Sci., 2014, 5, 424-436.
[47] JS Gómez-Jeria, Res. J. Pharmac. Biol. Chem. Sci., 2014, 5, 780-792.
[48] JS Gómez-Jeria; J Molina-Hidalgo, J. Comput. Methods Drug Des., 2014, 4, 1-9.
[49] JS Gómez-Jeria; J Valdebenito-Gamboa, Der Pharma Chem., 2014, 6, 383-406.

[50] F Salgado-Valdés; JS Gómez-Jeria, J. Quant. Chem., 2014, 2014 Article ID 431432, 1-15.
[51] R Solís-Gutiérrez; JS Gómez-Jeria, Res. J. Pharmac. Biol. Chem. Sci., 2014, 5, 1401-1416.
[52] MS Leal; A Robles-Navarro; JS Gómez-Jeria, Der Pharm. Lett., 2015, 7, 54-66.
[53] C Barahona-Urbina; S Nuñez-Gonzalez; JS Gómez-Jeria, J. Chil. Chem. Soc., 2012, 57, 1497-1503.
[54] DA Alarcón; F Gatica-Díaz; JS Gómez-Jeria, J. Chil. Chem. Soc., 2013, 58, 1651-1659.
[55] JS Gómez-Jeria; M Flores-Catalán, Canad. Chem. Trans., 2013, 1, 215-237.
[56] A Paz de la Vega; DA Alarcón; JS Gómez-Jeria, J. Chil. Chem. Soc., 2013, 58, 1842-1851.
[57] I Reyes-Díaz; JS Gómez-Jeria, J. Comput. Methods Drug Des., 2013, 3, 11-21.
[58] F Gatica-Díaz; JS Gómez-Jeria, J. Comput. Methods Drug Des., 2014, 4, 79-120.
[59] JS Gómez-Jeria, Int. Res. J. Pure App. Chem., 2014, 4, 270-291.
[60] JS Gómez-Jeria, Brit. Microbiol. Res. J., 2014, 4, 968-987.
[61] JS Gómez-Jeria, Der Pharma Chem., 2014, 6, 64-77.
[62] JS Gómez-Jeria, J. Comput. Methods Drug Des., 2014, 4, 38-47.
[63] D Muñoz-Gacitúa; JS Gómez-Jeria, J. Comput. Methods Drug Des., 2014, 4, 33-47.
[64] D Muñoz-Gacitúa; JS Gómez-Jeria, J. Comput. Methods Drug Des., 2014, 4, 48-63.
[65] DI Pino-Ramírez; JS Gómez-Jeria, Amer. Chem. Sci. J., 2014, 4, 554-575.
[66] JS Gómez-Jeria; A Robles-Navarro, Res. J. Pharmac. Biol. Chem. Sci., 2015, 6, 1337-1351.
[67] MJ Frisch; GW Trucks; HB Schlegel; GE Scuseria; MA Robb, et al., Gaussian98 Rev. A.11.3, Gaussian, Pittsburgh, PA, USA, 2002.
[68] JS Gómez-Jeria, D-Cent-QSAR: A program to generate Local Atomic Reactivity Indices from Gaussian log files. 1.0, Santiago, Chile, 2014.
[69] Statsoft, Statistica 8.0, 2300 East 14 th St. Tulsa, OK 74104, USA, 1984-2007.
[70] J Yang; R Yan; A Roy; D Xu; J Poisson; Y Zhang, Nat Meth, 2015, 12, 7-8.
[71] J Zhang; Y Zhang, Bioinformatics, 2010, 26, 3004-3005.
[72] GM Morris; R Huey; W Lindstrom; MF Sanner; RK Belew, et al., J. Comput. Chem., 2009, 30, 2785-2791.
[73] O Trott; AJ Olson, J. Comput. Chem., 2010, 31, 455-461.
[74] Accelrys Software Inc., Discovery Studio Visualizer 4.1, Accelrys Software Inc., San Diego, CA, USA, 2013.
[75] E Joselevich, ChemPhysChem, 2004, 5, 619-624.
[76] E Joselevich, Ang. Chem. Int. Ed., 2004, 43, 2992-2994.
[77] YC Martin, Quantitative drug design: a critical introduction, M. Dekker, New York, 1978.
[78] JS Gómez-Jeria; C Madrid-Aliste, J. Near Death Stud., 1996, 14, 251-272.